Superphénix Benchmark Part II: Transient Results

Ponomarev, A.; Mikityuk, K.; Fridman, E.; Di Nora, V. A.; Bubelis, E.; Schikorr, M.;

Originally published:

July 2021

Journal of Nuclear Engineering and Radiation Science 8(2022)1, 011321

DOI: https://doi.org/10.1115/1.4051877

SPX Benchmark Part II: Transient Results

A. Ponomarev[1], K. Mikityuk

Paul Scherrer Institute (PSI)

Forschungsstrasse 111, 5232 Villigen PSI, Schweiz.PSI

alexander.ponomarev@psi.ch, konstantin.mikityuk@psi.ch

E. Fridman, V. A. Di Nora

Helmholtz-Zentrum Dresden-Rossendorf (HZDR)

Bautzner Landstraße 400, DE-01328 Dresden, Germany

e-mail:e.fridman@hzdr.de, v.di-nora@hzdr.de

E. Bubelis, M. Schikorr

Karlsruher Institut für Technologie (KIT)

Hermann-von-Helmholtz-Platz 1, DE-76344 Eggenstein-Leopoldshafen, Deutschland

e-mail: evaldas.bubelis@kit.edu, michael.schikorr@kit.edu

[1] Corresponding author.

ABSTRACT

The paper presents a transient simulation phase of the new benchmark on a large sodium fast reactor core. This phase of the benchmark was devoted to the modelling of selected operational transients performed during start-up tests of French SFR Superphénix in order to evaluate its reactivity characteristics and core response to certain perturbations. Six operational transients were selected for the analysis. The specification of a simplified thermal hydraulic model equipped with point kinetics reactivity data and boundary conditions for the selected transients are given in the paper and the results of simulations with several system codes are reported. The study uses the results of the reference Serpent 2 Monte Carlo solution obtained during the first phase of the benchmark related to static neutronic characterization of the core. The developed model contains necessary thermal hydraulic description of primary system components and assumptions to account for thermal expansion reactivity feedbacks from in-reactor structures, neutron kinetics parameters, power distribution and reactivity coefficients. Thus the transient benchmark appears as an effective tool for validation and cross comparisons of system codes including approbation and comparison of different modelling features for thermal expansion of the in-reactor structures, giving a reference core behaviour with use of relatively simple models. The results of the modelling demonstrate a reasonable agreement between all solutions and with the experimentally measured evolution of the core parameters. Particular discrepancies with experimental data could not be resolved using the simplified benchmark model and available experimental data reconstructed from the published analysis of start-up tests. Because of that, the future steps for achieving the improved agreement between the simulated results and the experimental data were proposed.

ACRONYMS

1D	one-dimensional
GFR	Gas Cooled Fast Reactor
LWR	Light Water Reactor
MC	Monte Carlo
MOFC	Measurement of feedback coefficients
MOX	mixed uranium-plutonium oxide fuel
MSR	Molten Salt Cooled Reactor
IC	Inner core
IHX	Intermediate heat exchanger
OC	Outer core
PFS	Primary flow step
RB	Radial Blanket
RS	Reactivity step
SA	subassembly
SFR	Sodium cooled Fast Reactor
SG	Steam generator
SPX	Superphénix French sodium cooled fast reactor
SST	Self-stabilization test
US NRC	United States Nuclear Regulatory Commission

1. INTRODUCTION

The paper presents a second phase of the new large sodium fast reactor core benchmark [1] launched within the EU ESFR-SMART project [2]. This phase is devoted to transient simulation of the core of French Superphénix reactor at its start-up configuration. The paper provides the specification for transients modelling and results of modelling by three participants. It contains a description of the neutronics and thermal hydraulics core model for transient analysis including pin geometry, flow, power, reactivity and kinetics parameters, as well as boundary conditions for six selected transients. The specific power, reactivity and neutron kinetics characteristics of the core were evaluated within the first phase of the benchmark exercise [3].

The core configuration used is based on the core arrangement as has been achieved during start-up tests of the reactor [1]. Six operational transients were selected for the benchmark transient analysis of the core. Some of these transients relate to the experimental procedure of evaluation of

reactivity coefficients *k*, *g*, *h* [4]. The application of the TRACE and SIM-SFR codes for these transients already was reported in [5]. Practically this work aims also to reproduce these transients with one unified model as in [5], while using a different approach: (1) the model input parameters were revised on the basis of the Serpent 2 neutronics calculations results resulted from the Static neutronics phase [3]; (2) definitions of reactivity effects and the suggested set of effects were reconsidered based on results of modelling with Serpent 2 [6]; (3) proposed range of fuel-clad gap conductance values (in contrast to a more sophisticated approach with dynamic fuel pin mechanics in [5]) and range of CR position worth values in accord with power level and thermal core conditions [6].

The peculiarity of this work is application of one set of coefficients and approaches for modelling of wide range of power levels, as was already discussed during the benchmark preparation work [6]. As stated in [5], the aim of all plant transients at different power levels to be replicated with a single, unique reactivity coefficient set and without any further model/code changes makes this exercise significantly challenging and requires all pertinent feedback effects are understood and properly simulated. Recently a renewal of interest to the modelling of start-up tests can be stated [15, 16]. In particular a study to reproduce the conditions of RS transient, named as Negative Reactivity Insertion, is reported in [15].

The paper is structured as following. After given introduction, the second Chapter presents main core characteristics and choice of six selected transients. Chapter 3 contains the benchmark specification including all necessary thermal hydraulic, power, reactivity, kinetics data and temporal boundary conditions. The recommended parameters for modelling of in-reactor structures expansion and related feedbacks were selected as a result of preliminary model tests for considered transients. Chapter 4 presents a codes description along with peculiarities of modelling and code application which differ from the proposed benchmark specification. Chapter 5 summarises analysis of results obtained with TRACE, SIM-SFR and ATHLET codes. The transient phenomenology and discrepancies of modelling are discussed. Conclusions are given in Chapter 6.

2. SUPERPHENIX REACTOR CHARACTERISTICS AND SELECTED TRANSIENTS

Table 1 summarizes main parameters of the Superphénix reactor at nominal operation conditions and core description as achieved at start-up configuration.

Table 1. General characteristics of Superphénix reactor [20, 21]

Parameter	Value
Thermal/electric power	3000 / 1240 MW

Average fissile/fertile fuel temperature	1227/627 °C
Primary sodium inlet/outlet temperature, °C	395/545 °C
Primary sodium mass flow	16400 kg/s
Fissile/fertile fuel	$(U,Pu)O_2/UO_2$
Plutonium content in inner/outer core zones	16.0/19.7 %
Total mass of plutonium in the fissile core	5780 kg
Volume of the fissile core	10.8 m^3
Equivalent diameter of the fissile core	3.70 m
Height of the fissile pellet stack	1.00 m
Height of the lower/upper breeder blanket	0.30/0.30 m
Height of the radial blanket fertile pellet stack	1.60 m
Subassembly pitch in the diagrid	179.0 mm
Number of SAs in inner zone/outer zone/radial blanket	190/168/225
Number of control rods (CSD/DSD)	21/3

A number of experiments and tests were performed in order to evaluate the core thermal hydraulic and reactivity characteristics during start-up tests after the first criticality was achieved in 1985 [7]. Thus this benchmark exercise benefits from the experimental data evaluated from six operational transients which were reported in open literature, as it is introduced in [5]:

- MOFC1: -50 pcm reactivity insertion at 692 MWth;
- MOFC2: +10% secondary mass flowrate increase at 633 MWth;
- MOFC3: -10% primary mass flowrate reduction at 663 MWth;
- RS: -74 pcm stepwise reactivity insertion at 1542 MWth;
- PFS: -10% primary mass flowrate reduction at 1415 MWth;
- SST: +30 pcm reactivity insertion at hot zero power.

The description and reported experimental data for the first three transients (MOFC1-MOFC3) can be found in [4]. This report provides a detailed insight in the procedures of evaluation of reactivity characteristics of the core at different power levels resulted in experimental evaluation of the reactivity coefficients *k*, *g*, *h*. Despite of a relatively high uncertainty of the published experimental data, the three transients corresponding to three individual perturbations in the core

at around 650 MWth may serve as a fruitful basis for the codes and models calibration and are selected in the transient phase of the benchmark. In [8] three more transients are discussed in more detail in order to validate the project system code DYN, describing a sodium-cooled fast reactor. The report provides a comparison between calculation and experiment on the dynamic behaviour of the core alone and of the reactor as a whole. In particular, two transients (RS and PFS) demonstrate the core and whole system behaviour at close to 50% nominal power conditions, being a part of few step procedure for evaluation of reactivity coefficients at this power level. The comparisons were focused on global parameters such as neutronic power and sodium outlet temperature. While a detailed analysis of the individual reactivity contributions is also performed. Finally, a self-stabilization test (SST) was analysed characterized by a reactivity step at zero power. A satisfactorily agreement of calculation versus experiment on the dynamic behaviour of the core was stated using DYN code.

3. TRANSIENT BENCHMARK SPECIFICATION

A simplified primary system model proposed for the benchmark transient analysis is described hereafter. It comprises of three channels representing fuel subassemblies, inlet and outlet plena and pipes with boundary conditions, models of the primary system structures to account for their thermal expansions and related reactivity feedback effects, as well as a Point Kinetics model for prediction of power variation.

3.1. Core model overview

Thermal hydraulic domain of core model comprises three channels representing the subassemblies of inner core (IC), outer core (OC) and radial blanket (RB), connected to cold and hot plena (Fig. 1). The main approaches and characteristics of the model were developed in [6] and [9]. Boundary conditions at inlet pipe, specific for every transient, are defined by the transient variation of the inlet sodium temperature and mass flow rate. A constant pressure boundary condition of $1.5 \cdot 10^5$ Pa is imposed at outlet of the outlet pipe. The inlet and outlet pipes have length of 0.1 m and flow cross sections of 7.83 m^2 and 9.72 m^2, respectively. The core pressure drop at nominal power conditions is about $4.5 \cdot 10^5$ Pa. The sodium flow in the inter-subassembly gap is neglected. The inlet and outlet plenum is considered as a single mesh cell with four junction interfaces for 1D pipe components. Both plena have height of 0.1 m. Corresponding plena volumes are equal to 0.783 m^3 and 0.972 m^3, respectively for inlet and outlet ones.

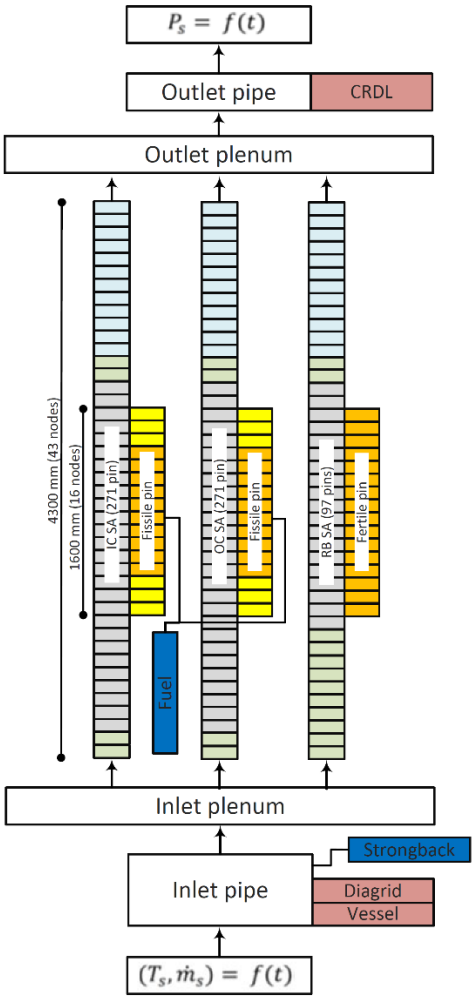

Fig. 1. Overview of the thermal hydraulic model.

3.2. Channel and plena parameters

3.2.1. Channel geometry and hydraulic parameters

The IC, OC, and RB dedicated channels include respectively 190, 168, and 225 SAs. Each individual channel represents all axial segments of the 4300 mm height subassembly. The fuel section is represented by one averaged pin. The channel and pin parameters are summarized in Table 2.

Table 2. The channel and pin parameters

Parameter	IC	OC	RB
Type of fuel	$(U,Pu)O_2$	$(U,Pu)O_2$	UO_2
Fuel burnup	fresh fuel	fresh fuel	fresh fuel
Stoichiometry	1.98	1.98	1.98
Number of SAs	190	168	225
Number of fuel pins in SA	271	271	91
Fuel pellet inner diameter*, mm	2.0	2.0	-

Fuel pellet outer diameter*, mm	7.14	7.14	14.36
Cladding inner diameter*, mm	7.37	7.37	14.66
Clad outer diameter*, mm	8.50	8.50	15.80
(*) corresponds to "as fabricated" dimensions			

The channel axial segments from the level of diagrid plate up to the outlet shielding sleeve are:

- the inlet section (empty hexcan);
- pin bundle represented by a single fissile or fertile pin (2700 mm or 1900 mm long, respectively) with associated heat structure for the fuel pellet stack height;
- upper flow transition section (empty hexcan);
- outlet shielding section (steel sleeve).

The hydraulic parameters and axial dimensions for different axial segments of the subassembly are listed in Table 3.

Table 3. Hydraulic parameters and axial representation of the channels

Parameter (fissile / fertile)	Axial section			
	Inlet section	Pin bundle	Upper transition section	Outlet section
Subassembly inner flat-to-flat size, m	1.651E-01			
Pin outer diameter, m	-	8.558E-03 / 1.591E-02	-	-
Number of fuel pins	-	271 / 91	-	-
Flow area, m2	2.361E-02	8.023E-03/5.525E-03	2.361E-02	3.848E-03
Hydraulic diameter, m	1.651E-01	4.084E-03/4.317E-03	1.651E-01	7.00E-02
Height, m-	0.2 / 1.0	2.7 / 1.9	0.2	1.2
Number of axial nodes	2/10	27 / 19	2	12

3.2.2. Power and flow conditions

Power distribution between channels and power axial profiles are given in Tables 4 and 5. The spatial distribution is fixed for all considered transients and does not vary with power level, as in accord to the Point Kinetics approximation.

Simplified SA flow gagging scheme with three cooling groups is established which corresponds to three core zones: IC, OC and RB. The cooling group mass flow rates were adjusted to achieve a similar average sodium heat-up of about 145°C in inner core and outer core at nominal operation conditions, while the sodium heatup in radial blanket subassemblies is set to somewhat lower value (up to 70°C in most powerful breeder SAs) [9]. The nominal primary mass flow rate is equal to 16400 kg/s. The mass flow rates for different channels are given in Table 5. For every

transient the mass flow rate was adjusted to reproduce the cooling conditions, i.e. in accord to experimentally measured sodium heatup.

Table 4. Power axial profiles for different channels

Axial layer	Height (bottom-to-top), cm		Axial profile, rel.		
	z-min	z-max	IC	OC	RB
1	0.0	10.0	1.349E-03	1.046E-03	1.337E-02
2	10.0	20.0	2.361E-03	1.909E-03	2.021E-02
3	20.0	30.0	5.228E-03	4.467E-03	3.570E-02
4	30.0	40.0	7.755E-02	7.589E-02	5.966E-02
5	40.0	50.0	9.907E-02	9.800E-02	8.194E-02
6	50.0	60.0	1.160E-01	1.153E-01	9.845E-02
7	60.0	70.0	1.257E-01	1.255E-01	1.086E-01
8	70.0	80.0	1.272E-01	1.274E-01	1.122E-01
9	80.0	90.0	1.203E-01	1.211E-01	1.092E-01
10	90.0	100.0	1.066E-01	1.081E-01	1.005E-01
11	100.0	110.0	8.971E-02	9.134E-02	8.691E-02
12	110.0	120.0	7.115E-02	7.240E-02	6.946E-02
13	120.0	130.0	5.214E-02	5.267E-02	4.898E-02
14	130.0	140.0	3.461E-03	3.048E-03	2.862E-02
15	140.0	150.0	1.444E-03	1.212E-03	1.583E-02
16	150.0	160.0	7.163E-04	5.905E-04	1.038E-02

Table 5. Power and mass flow distributions between channels

Parameter	IC	OC	RB
Power, MW	1.750E+09	1.208E+09	3.188E+07
Power fraction, rel.	0.5854	0.4039	0.0107
Mass flow rate, kg/s	9394	6481	525
Mass flow fraction, rel.	0.5728	0.3952	0.0320

3.2.3. Fuel-clad gap conductivity

The fuel-clad gap conductivity is highly uncertain. As a reference option, a simplified approach was proposed in the benchmark with fixed values, evaluated from the preliminary analysis of the considered transients with TRACE. In [6] application of the set of values depending on reactor power level has been proposed. This set, extended by values for zero power conditions, was used in the current benchmark study. Choice of the gap conductance parameter for every transient is given in Table 18.

3.3. Point kinetics neutronic model

The point kinetics approach is considered in the benchmark. The approach considers evaluation of individual reactivity contributions and total time dependent reactivity used in Point Kinetics equations to evaluate the transient power amplitude [6]. A detailed discussion on nature and importance of different contributions for this study of such a large core can be found also in [5].

3.3.1. Reactivity coefficients

The reactivity coefficients and parameters are summarized in Tables 6-10. The coefficients are provided without axial profile and thus are considered to be used with the core global or region-averaged parameter, i.e. fuel temperature and sodium temperature or density. Accounting for the axial profile of the Doppler Constant and sodium density coefficient was found nearly negligible for the given transients framework [9]. Table 10 collects data on alternative reactivity coefficients which were used in [5] in TRACE simulations for the analysis of these transients.

Table 6. Fuel Doppler Constant

Region	Doppler Constant, pcm
IC fissile	-757
OC fissile	-257
RB	-28
LAB	-54
UAB	-19
Total (as sum)	-1115

Table 7. Sodium density reactivity coefficient

	Sodium coefficient	
Region	pcm/°C	pcm/kg m^{-3}
Inner core	0.188	-0.896
Outer core	0.019	-0.096
Radial blanket	0.0	0.0
Total	0.207	-0.992

Table 8. Fuel axial expansion reactivity coefficient

Region	Fuel coefficient without account for CRs, pcm/°C	Fuel coefficient with CRs accounted for, pcm/°C
Inner core	-0.108	-0.184
Outer core	-0.084	-0.124
Radial blanket	0.0	0.0
Total	-0.192	-0.308

Table 9. Cladding and diagrid reactivity coefficients

Parameter	Value, pcm/°C

Cladding expansion coefficient	0.05
Diagrid radial expansion coefficient	-0.992

Table 10. Alternative definitions of some reactivity feedbacks as was considered in TRACE simulations in [5]

Parameter	Value
Strongback expansion coefficient, pcm/°C	-2.0
CRDL expansion coefficient, pcm/°C	-1.0
Vessel expansion coefficient, pcm/°C	4.0

3.3.2. Control rods position reactivity worth

The control rod position reactivity worth is another uncertain parameter for definition of the core state. It is dependent on realistic control rods curtains mutual position, on core power level and on inherent uncertainty of the evaluated value with respect to the experimentally observed one. An attempt to develop a simplified approach was done in [6]. The set of values corresponding to the core power level was proposed. The values were evaluated assuming needed compensation of the core reactivity at different power conditions following the CR worth curve obtained in [3]. Evaluated CR worth curve and CR position worth is given in Fig. 2. One should note, that this result differs from the worth curve reported in [10]. The peak value of CR position worth is somewhat lower than in [10] and shifted to the core bottom, and in the upper the part of the core the curve has a lower gradient in reverse to shape observed in [10], while the total CR worth of fully inserted CRs is well reproduced by the reference benchmark solution [1].

Taking into account the approaches proposed and results obtained in [6], as well as results of preliminary simulations of transients in order to verify the transient specification for the benchmark, the CR position worth parameter was defined as given below in Table 18, depending on individual core conditions for every transient.

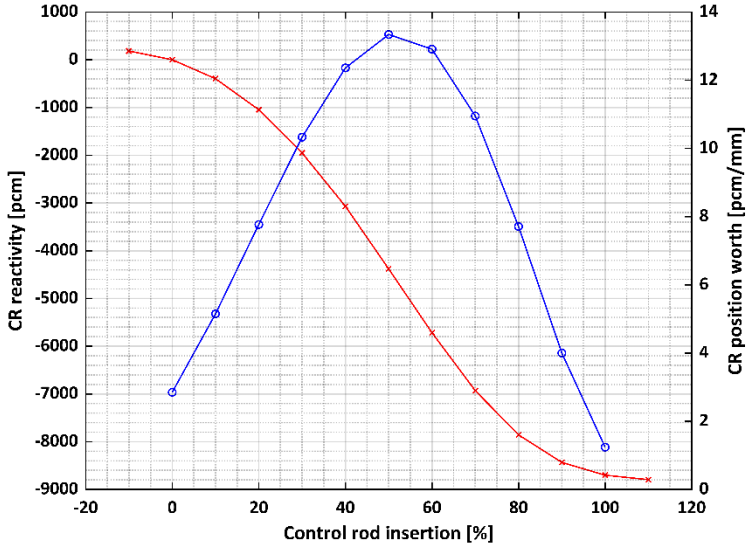

Fig. 2. Control rods reactivity and position worth versus insertion level as evaluated in [3] with Serpent 2 solution

3.3.3. Kinetic parameters

The neutron kinetics parameters are given in Table 11. This data was obtained with reference Serpent 2 solution in [3].

Table 11. Neutron kinetics parameters

Parameter	Value							
Prompt neutron lifetime, s	4.94E-07							
Effective delayed neutrons fraction, rel.	3.707E-03							
Group parameters:	1	2	3	4	5	6	7	8
Effective delayed neutrons fraction, rel.	6.165E-05	6.057E-04	2.251E-04	5.413E-04	1.170E-03	4.779E-04	4.197E-04	2.056E-04
Decay constant, s^{-1}	1.247E-02	2.829E-02	4.252E-02	1.330E-01	2.925E-01	6.665E-01	1.635E+00	3.555E+00

3.4. Structure thermal expansion models

The peculiarity of the proposed approach is application of simplified models of in-reactor structures to account for their thermal expansion and corresponding reactivity feedbacks. For all structural elements considered the axial elongation is of interest, except the diagrid plate for which the modelling of the radial expansion is required. The recommended parameters of different structures and their features obtained as result of the TRACE model calibration [6] were specified in the benchmark as presented hereafter.

3.4.1. Heat structures

3.4.1.1. Diagrid plate

The diagrid plate radial expansion is accounted following the core inlet temperature. The diagrid plate is represented by a 1D slab heat structure[2], with the parameters given in Table 12, which is connected to the sodium of inlet pipe. The average temperature of the diagrid heat structure drives the diagrid radial expansion reactivity effect.

Table 12. Diagrid plate heat structure parameters

Parameter	Value
Thickness, m	0.008
Thermal expansion coefficient, 1/°C	1.73E-05

3.4.1.2. Vessel

The vessel wall thermal expansion is taken into account driven by the core inlet temperature. To determine the average vessel temperature, driving the vessel wall elongation, the vessel heat structure is modelled as a 1D cylindrical heat structure with the wall thickness of 0.08 m (Table 13). Due to a complicated flow path of the sodium from the primary pump outlet to cool the vessel, evolution of the vessel temperature, which is used for the calculation of vessel length, is delayed by 360 s with respect to the predicted average temperature of the vessel heat structure. The vessel wall effective length is set to 13.5 m, as distance between the vessel connection to the slab and connection of the strongback to the vessel.

Table 13. Vessel and dedicated heat structure parameters

Parameter	Value
Effective length, m	13.5
Thermal expansion coefficient, 1/°C	1.70E-05
Inner radius, m	10.00
Outer diameter, m	10.08

[2] For diagrid, vessel and CRDL slab or cylindrical heat structures a negligibly small longitudinal dimension is considered to ensure no influence on the core inlet temperature as result of heat exchange

Time delay, s	360

3.4.1.3. Control rod drive line

The CRDL is modelled as a solid rod of effective length of 6.0 m (Table 14). The dedicated 1D cylindrical heat structure is connected to the sodium of outlet pipe. The change CRDL length is derived based on the average heat structure temperature, the effective length and thermal expansion coefficient (Table 14).

Table 14. CRDL and dedicated heat structure parameters

Parameter	Value
Effective length, m	6.0
Thermal expansion coefficient, 1/°C	1.70E-05
Inner radius, m	-
Outer radius, m	0.02

3.4.2. Models without heat structures

3.4.2.1. Strongback

The strongback structure parameters are given in Table 15. The change of the strongback height is considered driven by the core inlet temperature with delay of 100 s, as the strongback structure follows the temperature of the cold pool which is delayed with respect to the pump outlet or core inlet temperature. The effective height of the strongback structure (considered together with the diagrid plate) as the distance between its connection to the vessel and the bottom of the core is set to 4.0 m.

Table 15. The strongback parameters

Parameter	Value
Effective length, m	4.0
Thermal expansion coefficient, 1/°C	1.73E-05
Time delay, s	100

3.4.2.2. Fuel

The last component accounted for evaluation of the transient CR position change in the core is the change of fuel pellet stack height, as result of the fuel pellet thermal expansion. This contribution to the CR position change with respect to the fissile core is relatively uncertain. The same approach as implemented in [6] is proposed. The fuel related component is accounted for by considering the effective fuel length of 0.7 m and free expansion of MOX fuel (the open fuel-clad gap

is considered for the fresh fuel of the start-up core) driven by fissile fuel average temperature (Table 16).

Table 16. Parameters for fuel-related axial expansion contribution to CR position change

Parameter	Value
Effective length, m	0.7
Thermal expansion coefficient, 1/°C	1.30E-05

3.5. Materials

Materials of different core structural elements are listed in Table 17.

Table 17. Materials of different core structural elements

Parameter	Value
Pin cladding	316-Ti
CR drive line	Inconel-718
Diagrid plate	304L
Strongback	304L
Vessel	316L(N)/316SPX

3.6. Transients specification

In accord to transient individual core conditions (different power and primary mass flow rate) a transient specification was developed and tested for the benchmark with use of TRACE. In the Table 18, the recommended parameters of the model are listed for every simulated transient. Accordingly, a specific external reactivity, core inlet sodium temperature and mass flow boundary conditions are presented in subsequent Chapters 3.6.1-3.6.6.

Table 18. Specification for transients

Parameter	MOFC1	MOFC2	MOFC3	RS	PFS	SST
Reactor power, W	6.920E+08	6.333E+08	6.632E+08	1.540E+09	1.415E+09	8.500E+04
Total IC power, W	4.051E+08	3.708E+08	3.883E+08	9.016E+08	8.284E+08	4.976E+04
Total OC power, W	2.795E+08	2.558E+08	2.679E+08	6.220E+08	5.715E+08	3.433E+04
Total RB power, W	7.378E+06	6.752E+06	7.071E+06	1.642E+07	1.509E+07	9.062E+02
IC average pin power, W	7.868E+03	7.200E+03	7.540E+03	1.751E+04	1.609E+04	9.664E-01
OC average pin power, W	6.139E+03	5.618E+03	5.884E+03	1.366E+04	1.255E+04	7.541E-01
RB average pin power, W	3.603E+02	3.298E+02	3.453E+02	8.019E+02	7.368E+02	4.426E-02
Fissile gap conductance, $W \cdot m^{-2} \cdot K^{-1}$	2800	2800	2800	6000	6000	1500
Fertile gap conductance, $W \cdot m^{-2} \cdot K^{-1}$	2400	2400	2400	5000	3500	1100

Initial inlet coolant temperature, C	389.0	384.9	374.2	399.7	383.0	179.0
Initial coolant flowrate, kg/s	6300	6360	6300	10400	10400	3200
CR position worth, pcm/mm	12.0	12.0	12.0	0.9	0.9	14.0

3.6.1. MOFC1: -50 pcm reactivity insertion at 692 MWth

As specified in the Introduction, the MOFC1 transient was initiated as a first step of the three-step procedure for evaluation of *k*, *g*, *h* reactivity coefficients at power level of about 650 MWth (~20% nominal). The data reported in [4] was used for constructing the input data for the benchmark. It is worth to mention, that the corresponding calculation experiments were modelled in [6] using TRACE model for similar core conditions.

For the benchmark definition, the insertion of 50 pcm negative reactivity at power of 692 MW was considered as in accord to Table 19. Transient time start is set to *t*=250 s. The inlet sodium temperature (Table 20) varies in accord to data reconstructed from [4], as no response of secondary circuit is modelled. Primary mass flow equal to 6300 kg/s (see Table 18) was adjusted to have a sodium heatup of ~83°C prior to the transient and is considered to be constant during the transient.

Table 19. External reactivity insertion in MOFC1

Time, s	Inserted reactivity, pcm
0.0	0.0
250.0	0.0
252.0	-50.0
3000.0	-50.0

Table 20. Core inlet sodium temperature in MOFC1

Time, s	Core inlet temperature, °C
0.0	389.0
400.0	389.0
565.4	388.1
720.2	387.0
865.1	386.4
1010.5	386.2
1187.3	386.3
1353.4	386.1
1613.0	385.8
1799.9	385.6

2059.9	385.7
2288.5	385.6
2506.6	385.3
3000.0	385.3

3.6.2. MOFC2: +10% secondary mass flowrate increase at 633 MWth

Following the MOFC1, the MOFC2 is the second step of the procedure for evaluation of reactivity coefficients, where secondary mass flow rate was perturbed [4]. The increase of the secondary mass flow rate, initiated at *t*=250 s, results in enhanced heat removal from the primary sodium and corresponding decrease of the core inlet temperature (Table 21), which is the only time dependent boundary condition in the benchmark definition of this transient. The sodium heatup of ~75°C is achieved at steady state prior to the secondary flow perturbation with the primary flow of 6350 kg/s.

Table 21. Core inlet sodium temperature in MOFC2

Time, s	Core inlet sodium temperature, °C
0.0	384.9
250.0	384.9
310.9	383.4
350.7	381.6
442.5	379.9
565.7	378.4
710.0	377.2
865.2	376.5
1073.1	376.4
1311.7	375.9
1581.6	375.6
1831.0	375.5
2101.2	375.3
2350.5	375.1
2620.4	374.7
2953.0	374.6
3000.0	374.4

3.6.3. MOFC3: -10% primary mass flowrate reduction at 663 MWth

The MOFC3 transient is the third and the last step of the three-step procedure. The primary mass flow is adjusted to 6300 kg/s to obtain the sodium heatup of ~79°C at steady state. The decrease of the primary flow by 10% is considered as perturbation at *t*=250 s (see Table 22).

Variation of the primary flow results in variation of the core inlet temperature as in accord to Table 23.

Table 22. Primary flow in MOFC3

Time, s	Mass flow rate, rel.
0.0	1.0
250.0	1.0
325.0	0.9
3000.0	0.9

Table 23. Core inlet sodium temperature in MOFC3

Time, s	Core inlet temperature, °C
0.0	374.2
300.0	374.2
370.7	372.1
410.4	370.2
440.5	369.1
626.7	368.3
844.6	367.9
1145.9	367.7
1457.4	367.3
1852.1	366.9
2278.0	366.6
2631.3	366.4
2963.7	366.2
3000.0	366.1

3.6.4. RS: -74 pcm stepwise reactivity insertion at 1542 MWth

The RS transient reported in [8] is a first step of the three step procedure to evaluate reactivity coefficients at power level close to 50%. The reactivity insertion of -74 pcm is considered as prescribed by Table 24. Some experimentally achieved divergence from steady state conditions is reflected in the input on sodium inlet temperature. The transient start time is set to *t*=300 s, followed by initiation of first CR insertion at *t*=600 s. The core inlet temperature exhibits a somewhat wavy behaviour which was also taken into account in the benchmark specification (Table 25). Initial primary mass flow was adjusted to value of 10050 kg/s to ensure the sodium heatup of 117°C prior to the transient.

Table 24. External reactivity in RS

Time, s	Inserted reactivity, pcm
0.0	0.0
600.0	0.0
602.0	-25.0
660.0	-25.0
662.0	-50.0
720.0	-50.0
722.0	-74.0
3500.0	-74.0

Table 25. Core inlet sodium temperature in RS

Time, s	Core inlet temperature, °C
200.0	399.7
302.0	399.7
348.3	399.5
411.8	399.4
475.5	399.1
556.6	398.7
654.7	398.6
712.4	398.5
787.8	398.0
898.1	397.0
985.2	396.2
1049.2	395.5
1130.6	394.6
1211.9	393.8
1241.0	393.4
1281.5	393.2
1351.1	392.7
1507.0	392.5
1581.8	392.8
1656.9	392.7
1685.8	392.6
1708.8	392.7
1743.5	392.6
1829.9	392.9
2003.5	392.0
2084.2	392.1
2165.0	392.1
2245.7	392.2
2320.8	392.0
2378.5	392.0
2447.8	392.0
2482.2	392.3

2637.8	392.6
2672.5	392.3
2724.5	392.3
2770.8	392.1
2845.9	391.9
2915.2	391.8
2955.4	392.0
3059.3	392.0
3117.1	391.8
3157.5	391.9
3186.4	391.7
3278.6	391.8
3341.9	392.1
3500.0	392.1

3.6.5. PFS: -10% primary mass flowrate reduction at 1415 MWth

The analysis of the PFS transient can be found in [8]. It belongs to the procedure of evaluation of reactivity coefficients at ~50% nominal power. The steady state primary mass flow rate is equal to 10020 kg/s, resulting in the initial sodium heatup of ~107°C. The perturbation of the primary flow, introduced at *t*=450 s, resulted in flow decrease by 11.5% as prescribed in Table 26. Core inlet temperature variation is given in Table 27.

Table 26. Mass flow rate in PFS

Time, s	Mass flowrate, rel.
0	1.0
450	1.0
750	0.890
1000	0.885
3500	0.885

Table 27. Core inlet sodium temperature in PFS

Time, s	Core inlet temperature, °C
0.0	383.0
450.0	383.0
456.8	382.9
512.8	382.2
532.7	381.4
534.4	380.7
541.7	380.1
556.0	379.2

563.8	378.4
577.1	377.9
603.2	377.1
623.4	376.1
661.1	375.5
692.6	374.9
736.3	374.3
791.2	374.0
845.2	374.2
911.0	374.5
976.7	374.7
1005.8	375.2
1053.9	375.3
1126.7	375.1
1199.9	374.8
1297.7	374.3
1370.6	374.1
1545.6	374.1
1624.5	373.9
1679.7	373.6
1765.3	373.1
1850.5	372.7
1959.5	372.6
2092.0	372.8
2254.7	372.9
2382.2	372.5
2443.3	372.2
2552.4	372.0
2666.3	372.4
2774.5	372.6
2876.6	372.8
2985.3	372.8
3094.6	372.5
3203.9	372.2
3288.6	372.1
3500.00	372.1

3.6.6. SST: +30 pcm reactivity insertion at hot zero power

The information on the reactivity step at zero power level, or self-stabilization test, is given in [8]. Prior to this transient, the reactor is critical at zero power at steady state isothermally heated up to 179°C conditions. Initial sodium heatup is close to zero. The reactivity of 30 pcm (~0.1$) was inserted by the partial withdrawal of a control rod (Table 28) at *t*=500 s. During the transient, a variation of the inlet temperature was also observed as prescribed in Table 29, which results in

different thermal feedbacks complementing the negative fuel Doppler effect feedback, what allows to mitigate the reactor power rise and achieve new stabilized conditions.

Table 28. External reactivity in SST

Time, s	Inserted reactivity, pcm
0.0	0.0
500.0	0.0
502.0	30.0
3500.0	30.0

Table 29. Core inlet sodium temperature in SST

Time, s	Core inlet temperature, °C
0.0	179.1
500.0	179.1
600.0	179.1
1400.0	179.1
1696.1	179.1
1893.6	179.3
2132.7	179.5
2461.5	179.8
2718.5	180.1
3041.7	180.3
3377.7	180.4
3500.0	180.5

4. Codes and modelling features

4.1. TRACE

The modified version of US NRC TRACE code was used which includes modifications of sodium two-phase flow option, fast reactor specific reactivity effects embedded in PARCS neutronics solver, new fuel performance model, etc. [11]. The code was extensively applied in the past for analysis of a different innovative reactor types (SFR, GFR, MSR) [12].

The TRACE model was built following the detailed benchmark specification. The model features were preliminary tested for evaluation of SPX core characteristics and transient behaviour in [6] and [9]. The Point Kinetics model developed in [6] was utilised in the benchmark simulations.

4.2. SIM-SFR

The SIM-SFR code is a reactor simulator which was actively used to analyse different reactor types and designs in the past [13, 14]. A simplified SPX model was developed in [5] for study of six transients selected in the benchmark.

All fuel assemblies of the inner and the outer core zones of the SPX core are modelled by an average power and a peak power fuel assembly. That means that two fuel channels are being modelled in SIM-SFR for the fuel assemblies' part, plus a bypass channel for all the other non-fuel channels of the reactor core. Axially the active core is modelled in 16 axial neutronically and thermohydraulically coupled meshes. Apart from the core, modelled are primary, secondary and tertiary cooling circuits, including the intermediate heat exchangers (IHX) and pumps, and the steam generators (SG). Feedwater supply to the SGs is modelled as a boundary condition, assuming constant operational parameters. The following reactivity feedback effects were modelled: Doppler, fuel and clad axial expansion, diagrid radial expansion, coolant expansion and control rod driveline (CRDL) axial expansion.

All reactor design, thermal-hydraulic and neutronic parameters of SPX were taken from the official benchmark specification. The first difference from the benchmark specification is that in SIM-SFR simulations the Doppler constant was taken equal to -890 pcm, instead of the calculated benchmark value of -1115 pcm. The reason for this being that, when using the Doppler constant of -890 pcm, SIM-SFR results are being obtained to be rather close to the complete set of experimental transient data sets. The second difference is that fuel-clad gap conductance values, as proposed in Table 18, were not taken into account. Instead, the dynamic fuel-clad gap model implemented in SIM-SFR was used in the simulations. The third difference is that a dynamic CRDL expansion model is used as implemented in SIM-SFR code, instead of the benchmark recommendation for CRDL expansion, as presented above. The fourth difference between SIM-SFR and TRACE codes lays in the modelling of the vessel thermal expansion reactivity effect (for details refer to Ref. [5]). For the benchmark simulations the mass of the reactor vessel for heat redistribution and radiation heat loss from the reactor vessel to the ambient have been taken into account as well.

4.3. ATHLET

The ATHLET code [17] is a thermal hydraulic computational tool developed by GRS equipped with a general control simulation module and point kinetics model. The code, extensively applied to the modelling of Light Water Reactors (LWRs), was recently extended to account for liquid sodium properties [18]. Although under verification and validation, the extension opens up to the possibility of modelling SFR systems. Such a possibility was already exploited for a verification exercise in [19]. In fact, ATHLET was already applied, with a simplified two channels mock-up, to the modelling of the SPX start-up tests and benchmarked against TRACE providing promising outcomes.

The existing mock-up was upgraded to be consistent with the current benchmark specifications and then applied to this study. In particular, the model includes now three main core channels, modelled as described in section 3.2., a more detailed point kinetics model accounting for

several core regions (i.e. IC, OC, RB, and axial blankets), as well as, a control block for the modelling of expansion of out-of-core structures specified in section 3.4. Fuel pellet stacks are represented by three averaged pin models, one per hydraulic channel, for the full 1.6 m length of the stack. Average core-region-wise fuel temperatures were explicitly computed by averaging fuel temperatures in pin layers.

The ATHLET model was conceived to be equivalent to the TRACE model, comparable outcomes are thus expected. Discrepancies can nevertheless arise from different heat transfer models and correlations and material properties used by the models and codes.

5. TRANSIENT SIMULATIONS RESULTS

Every transient was initiated after the reactor reaches fully stabilized thermal conditions (steady state) at prescribed power level. This is essentially important for modelling of in-reactor structures for which a considerable simulation time is required even with the considered simplified model to achieve thermal equilibrium conditions. Depending on transient definition, the model is equipped with individual parameters given in Table 18. All other parameters, such as the features of heat structures, are fixed for all transients.

5.1. MOFC1: -50 pcm reactivity insertion at 692 MWth

In MOFC1 transient, the negative reactivity of -50 pcm is introduced by a CR insertion when the reactor was stabilized at 692 MWth. Selected results of simulations by three codes are visualized in Fig. 3-9. In Fig. 3 the predicted evolution of the reactor power is given along with the estimated from [4] experimental data. A reasonable agreement is observed between all solutions (within ~10 MW) and with the experimental data. After insertion of negative reactivity, the transient is driven by strong positive contributions of Doppler and fuel axial expansion (Fig. 4) due to decrease of the bulk fuel temperature. These are complemented by an additional positive reactivity due to CRDL contraction, as a result of sodium heatup decrease and corresponding cooling down of the CR drive lines, as depicted in Fig. 5 and 6, where evolution of the core heatup, core outlet and CRDL temperatures is shown. As a result of the accurate prediction of the power evolution, the heatup evolution was also predicted with appropriated agreement within about 1°C. Some differences are observed in prediction of the CRDL temperature and corresponding reactivity between SIM-SFR and other two solutions of TRACE and ATHLET. SIM-SFR predicts a stronger decrease of the CRDL temperature while the corresponding reactivity effect is less pronounced (by ~0.25). The reason for this might be related to different CRDL models between the codes and thus the resulting CRDL reactivity effect.

By modelling approach, the reactivity feedbacks of diagrid, strongback and vessel are linked to the pre-defined input core inlet temperature, which is plotted in Fig. 7, thus depend on this

parameter and inherent modelling features only and do not depend on transient reactivity and power conditions. One can see, that the diagrid temperature is nearly following the core inlet temperature thus introducing a noticeable positive reactivity after about 250 s (Fig. 4). Two other effects are acting opposing to each other: contraction of the strongback, as result of the temperature decrease results in a withdrawal of CRs, while vessel wall contraction, which occurs with considerable delay, results in a delayed insertion of CRs into the core. Resulting change of CRs position in the core predicted by TRACE is depicted in Fig. 8 (the initially inserted negative reactivity is not modelled by CR position change and is not accounted for in CR position change plotted). The corresponding decrease of the CR position related positive reactivity is observed after ~600 s of the transient (Fig. 4).

Differences are observed in the amplitude of the sodium density reactivity effect (Fig. 4). The reason may lay in the use of different core models between the codes, as well as somewhat different value of the sodium temperature, that was taken in the codes models as the driving temperature for the sodium density reactivity effect. This effect does not influence the results significantly due to a limited magnitude of the effect. Particular differences were observed in evaluation of steady state and transient core-average fuel temperatures, as can be seen in Fig. 9. The absolute differences between the values at steady state are rather small (below 30°C). These differences can be attributed to different pin heat transfer modelling. In particular, SIM SFR uses one averaged pin to reproduce both inner and outer core, while TRACE and ATHLET models use two individual channels. As can be seen from Fig. 4, these fuel temperature differences do not result in noticeable deviations in prediction of the fuel Doppler reactivity.

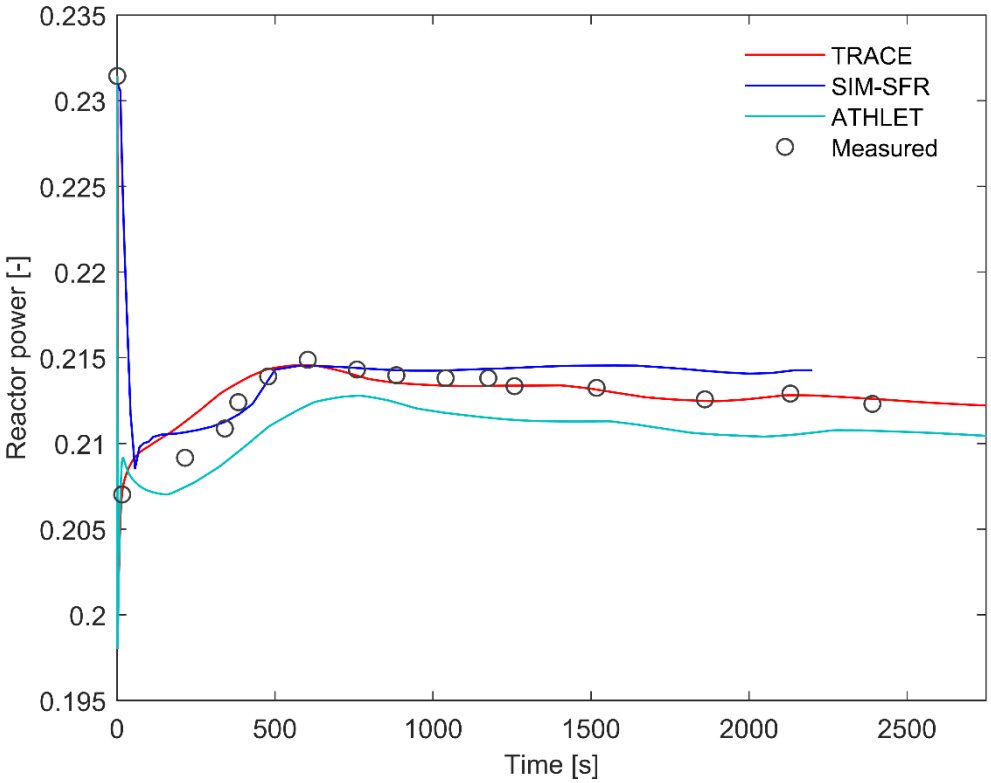

Fig. 3. Reactor power evolution in MOFC1 transient

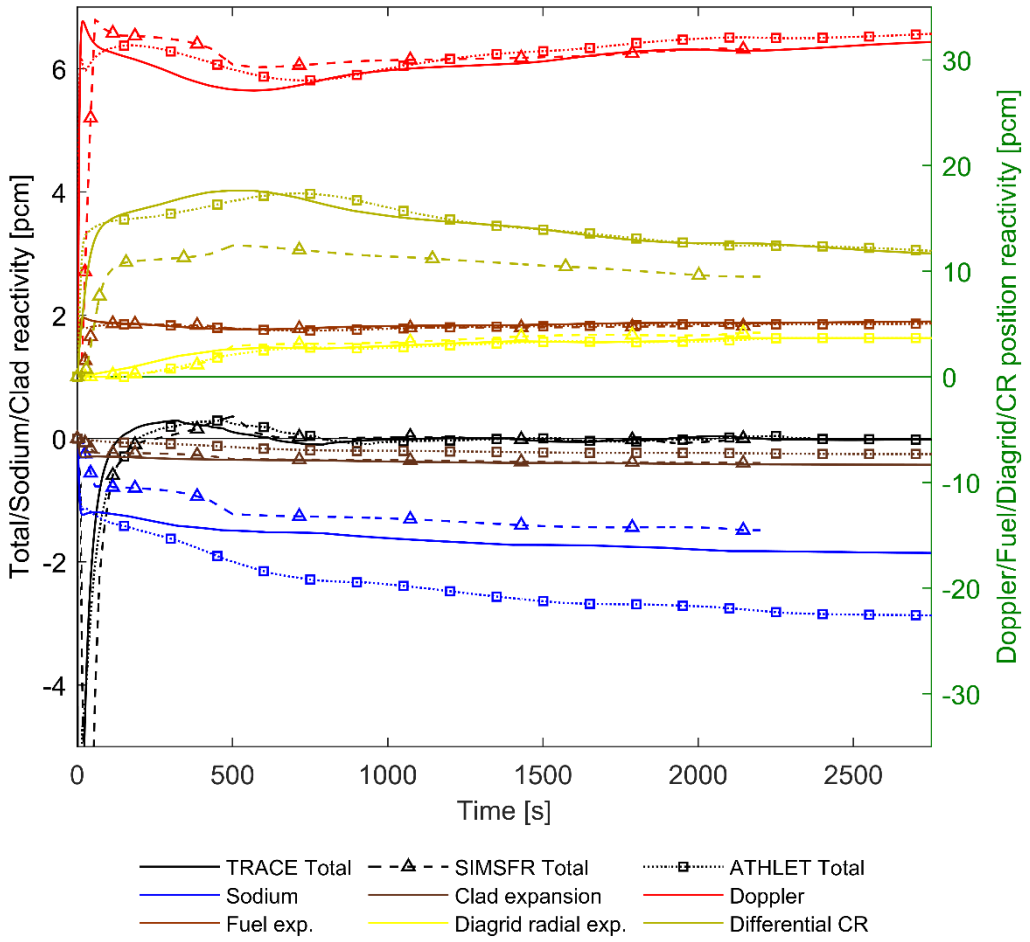

Fig. 4. Core reactivity and its decomposition during MOFC1 transient predicted by different codes (total, sodium density and clad expansion reactivity refer to Y-axis to the left; and Doppler, fuel axial expansion, diagrid radial expansion and CR position reactivity refer to Y-axis to the right)

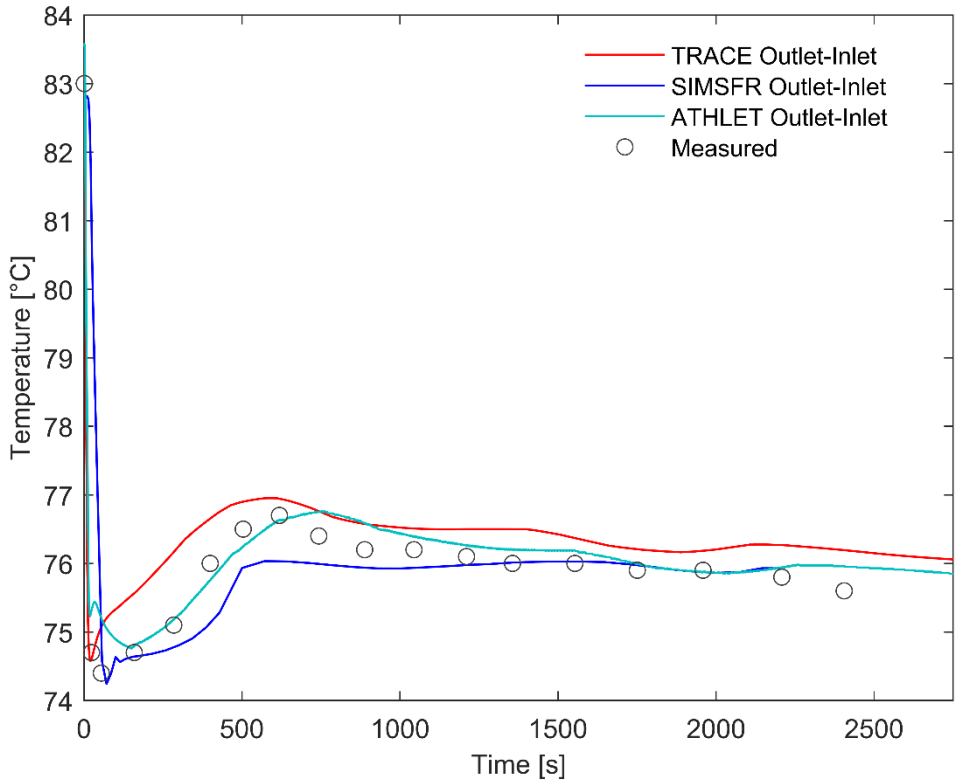

Fig. 5. Sodium core heatup in MOFC1 transient

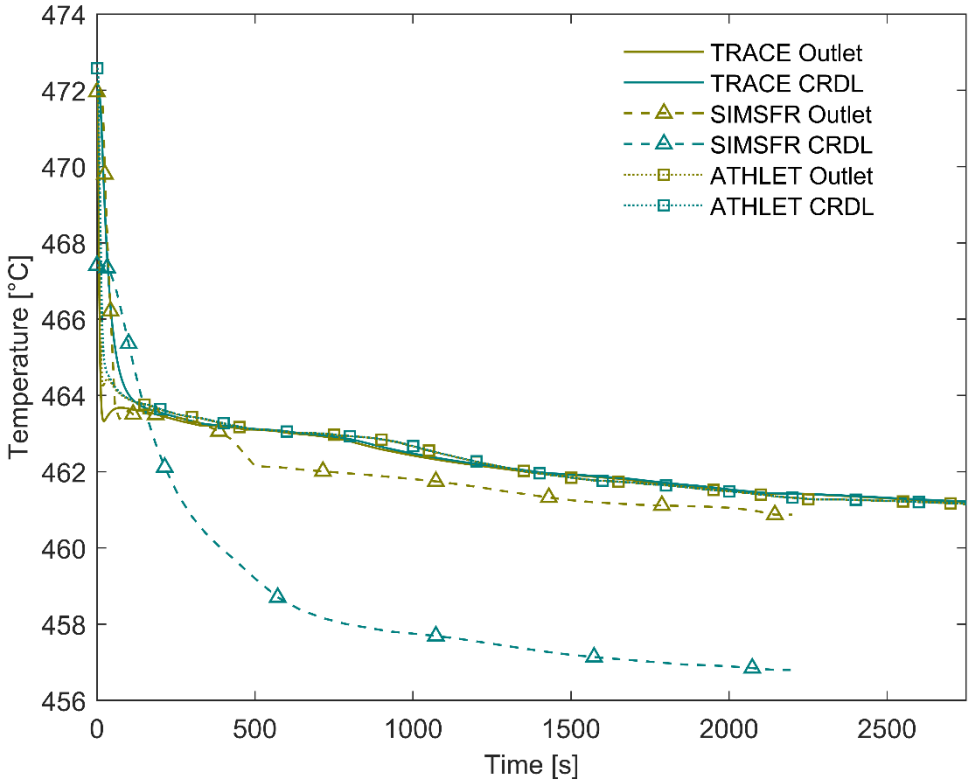

Fig. 6. Core outlet and CRDL temperatures during MOFC1

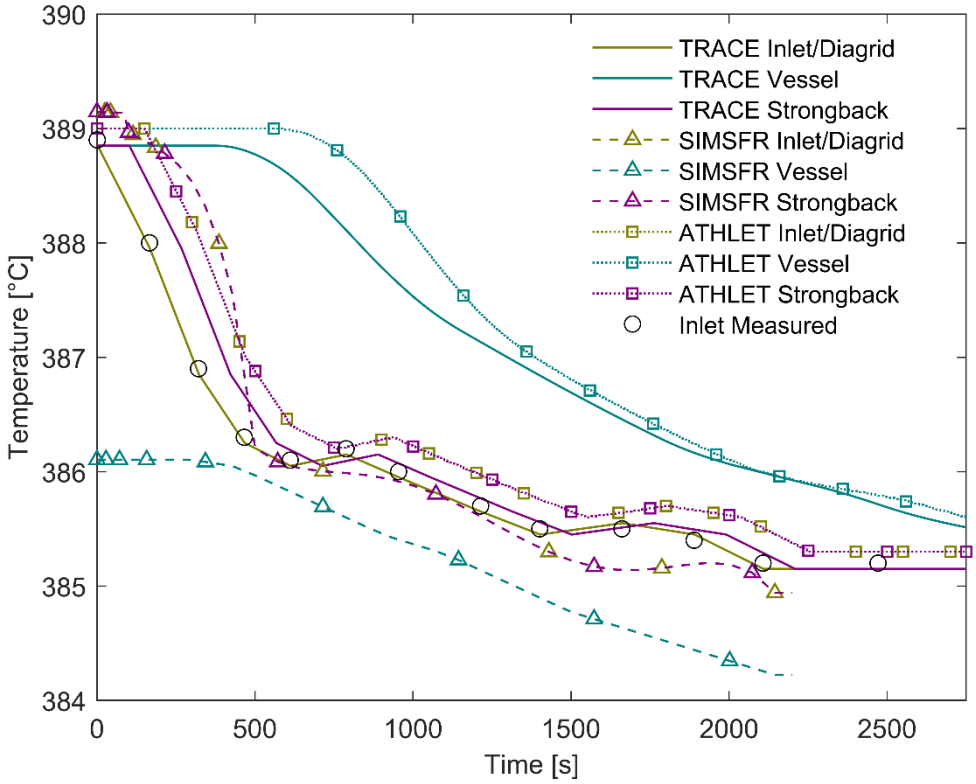

Fig. 7. Core inlet, diagrid plate, strongback, vessel temperatures during MOFC1 transient

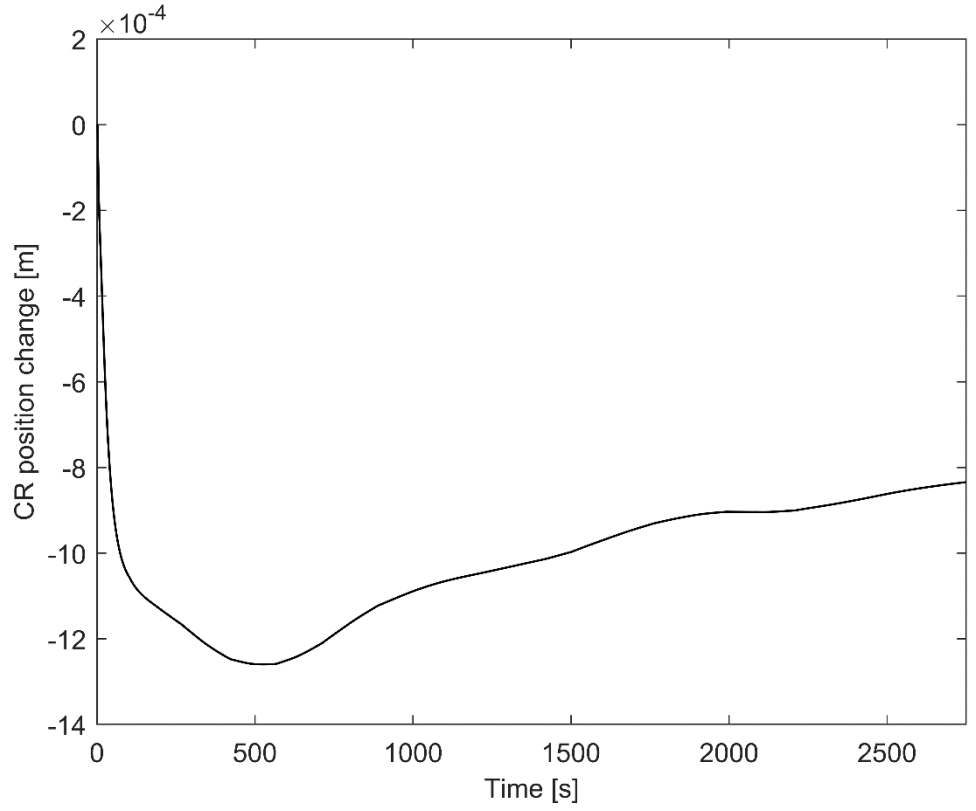

Fig. 8. CR position change during MOFC1 as predicted by TRACE code
(negative value corresponds to CRs withdrawal)

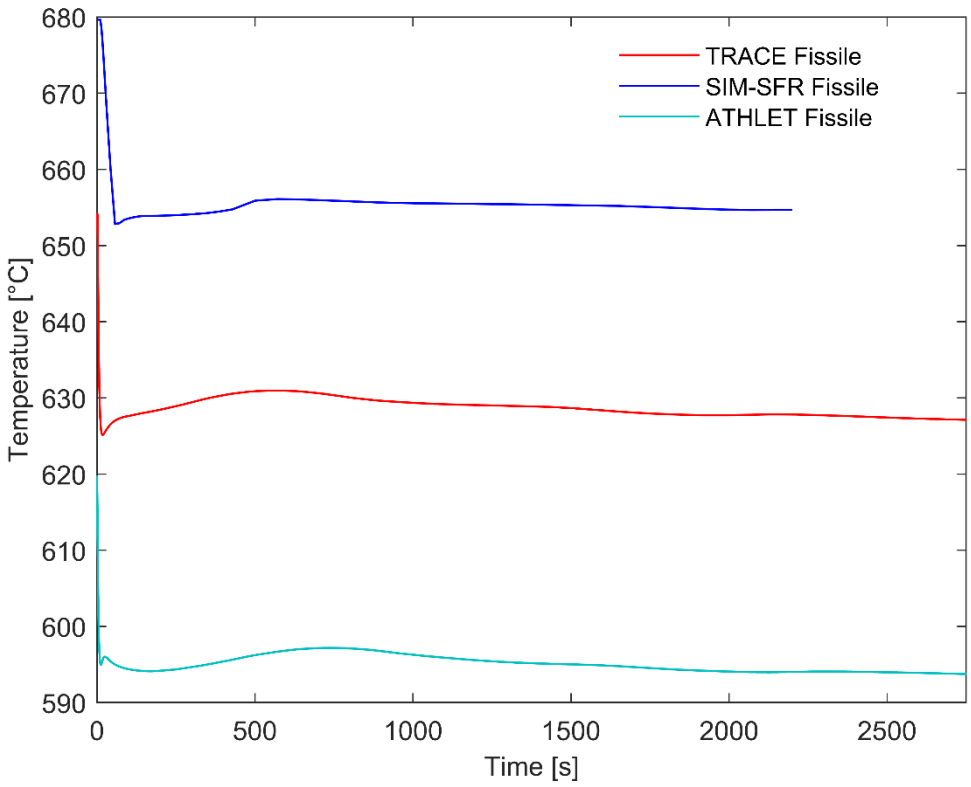

Fig. 9. Core-averaged fissile fuel temperature during MOFC1 transient

5.2. MOFC2: +10% secondary mass flowrate increase at 633 MWth

As the reactor stabilized at 633 MWth, the secondary mass flow increase by 10% was initiated. Evolution of the selected parameters predicted by the three codes is given in Figs. 10-16. As the core inlet temperature decrease is the only initiator in this transient, a nearly immediate diagrid positive reactivity is inserted, leading to core power rise, while the fuel Doppler effect tends to counterbalance this effect (Fig. 11). Despite of the power increase, the core outlet sodium temperature decreases, resulting from a more pronounced decrease of the core inlet temperature (see Fig. 12 and 13). The change of core inlet temperature reaches ~9°C after first ~500 s while the predicted sodium heatup is smaller, about 5°C (Fig. 14). Thus this initial contraction of CRDL accompanied by contraction of the strongback and corresponding withdrawal of CRs (Fig. 15) results in insertion of additional positive reactivity of up to ~8 pcm after first ~500 s (see Fig. 11 and Fig. 15). After 500 s the power rise is followed by decrease and tend to stabilization as a result of a strong contribution of the vessel expansion related reactivity (approaching -30 pcm at the end of simulation time, as predicted by TRACE).

TRACE and ATHLET simulation results exhibit close agreement within ~4 MW between each other as well as with evaluated experimental data (below ~8 MW) regarding the power transient variation (Fig. 10). This agreement is also reflected in coherent prediction of sodium core heatup (within 1°C for the whole simulation time range). The temperature of the vessel which is used for calculation of actual vessel height is nearly identically reproduced by two models. (Fig. 13). The cumulative CR position reactivity is very close to the one in TRACE simulations. This reactivity seems to be overestimated with the given model features resulting in a deeper power decrease up to the end of simulation time. Somewhat larger discrepancy in evaluation of sodium density effect between TRACE and ATHLET as compared to the MOFC1 scenario is observed for MOFC2 transient, due to a stronger sodium heatup predicted by ATHLET. The same way, this reactivity contribution does not influence noticeably the transient reactivity evolution.

Results of SIM-SFR differ from those of TRACE and ATHLET. The power rise is smoother with the lower peak value and stabilization is also smoother being closer to the experimental data at the end of simulation time as compared to the two other solutions. This power difference results in a difference in evaluation of core heatup of up to 1.5°C at point of power maximum. The main reactivity contributions of Doppler and CR position effect are smaller in magnitude. Different modelling features result in somewhat different behaviour of vessel and CDRL temperatures and corresponding evolution of CRDL and vessel reactivity feedbacks. Overall, the reactivity balance stays similar for all three codes. The discrepancies of the same level of magnitude are observed for the fuel temperature (Fig. 16).

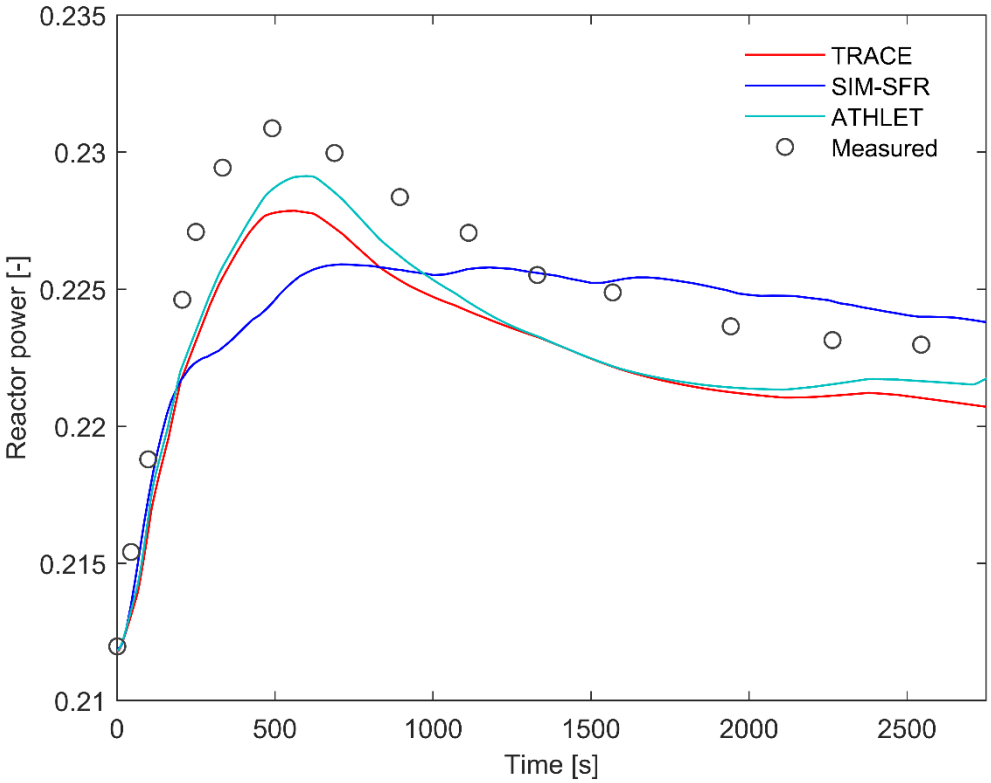

Fig. 10. Reactor power evolution in MOFC2 transient

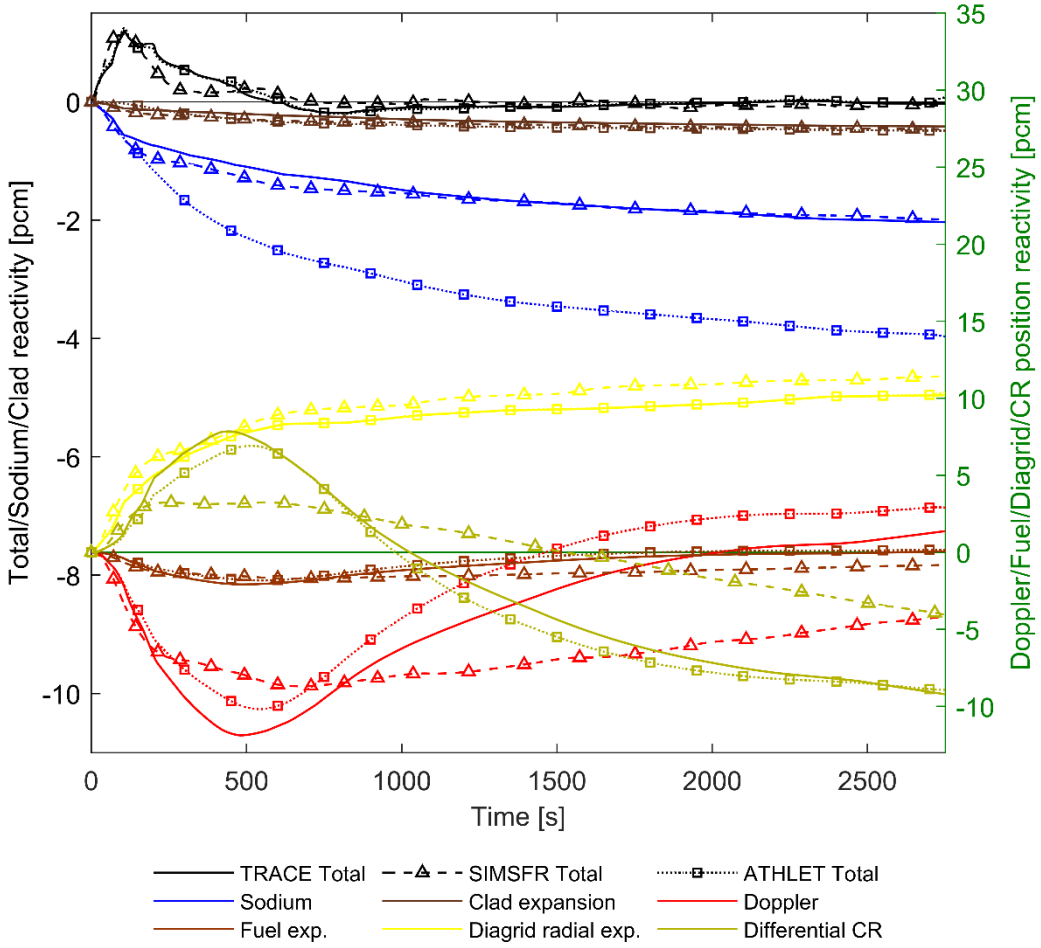

Fig. 11. Core reactivity and its decomposition during MOFC2 transient predicted by different codes (total, sodium density and clad expansion reactivity refer to Y-axis to the left; and Doppler, fuel axial expansion, diagrid radial expansion and CR position reactivity refer to Y-axis to the right)

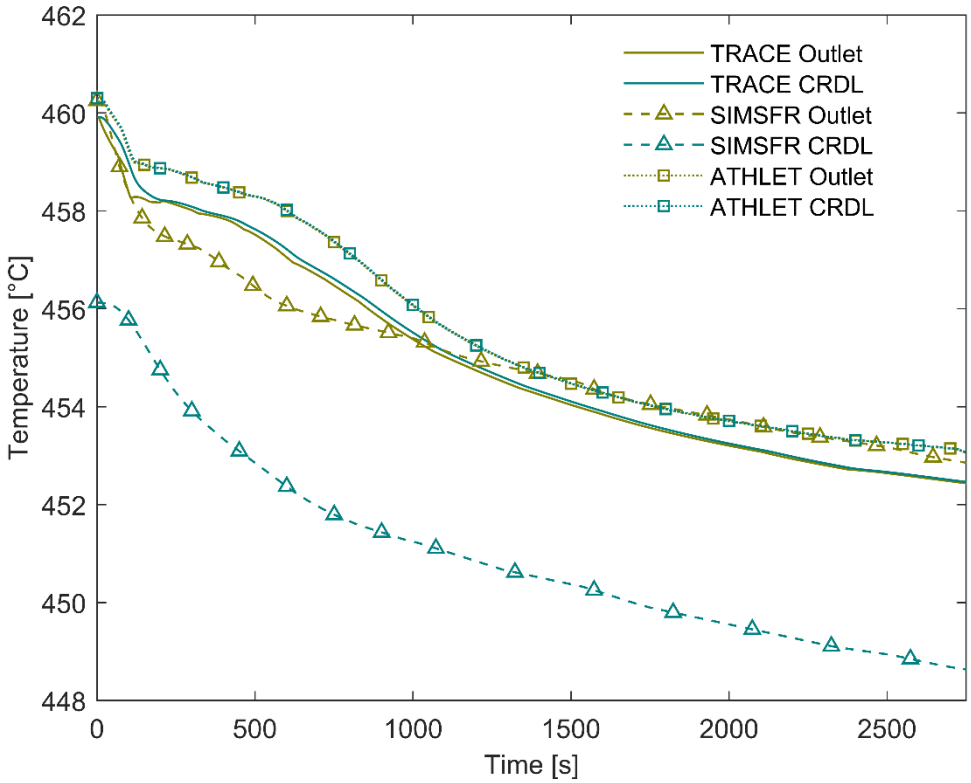

Fig. 12. Core outlet and CRDL temperatures during MOFC2

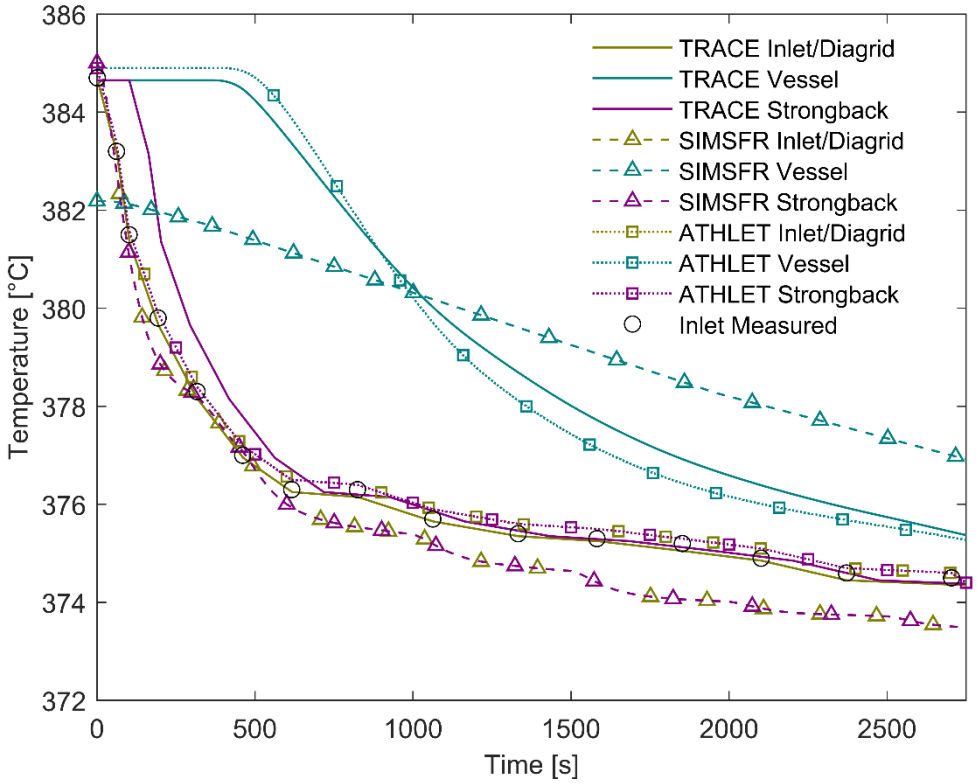

Fig. 13. Core inlet, diagrid plate, strongback, vessel temperatures during MOFC2 transient

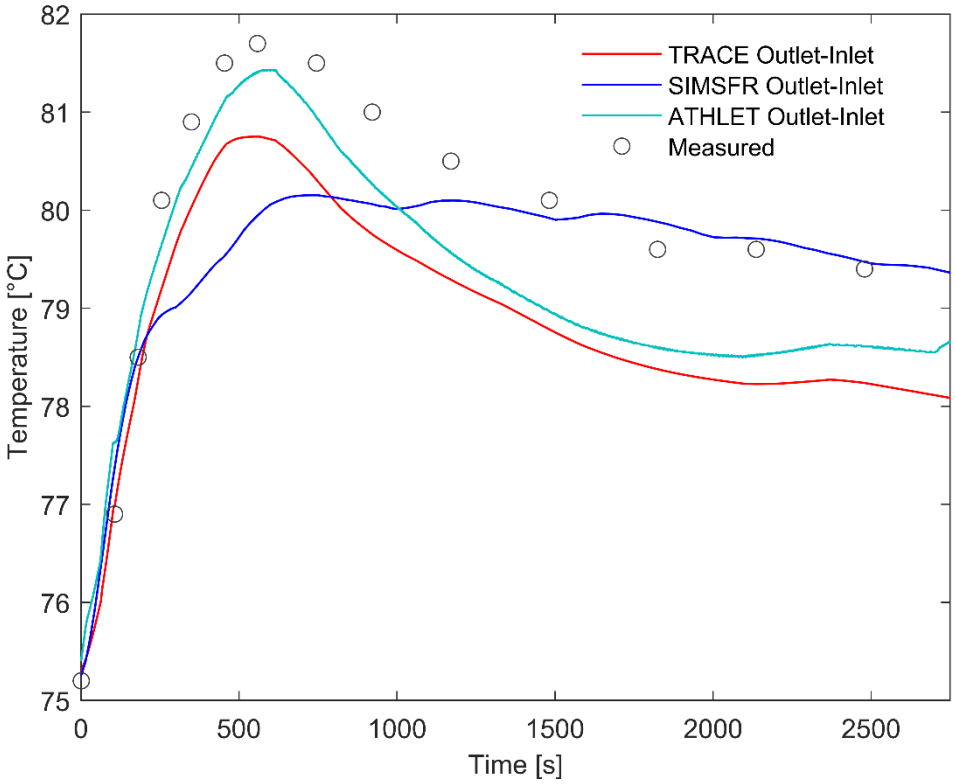

Fig. 14. Sodium core heatup in MOFC1 transient

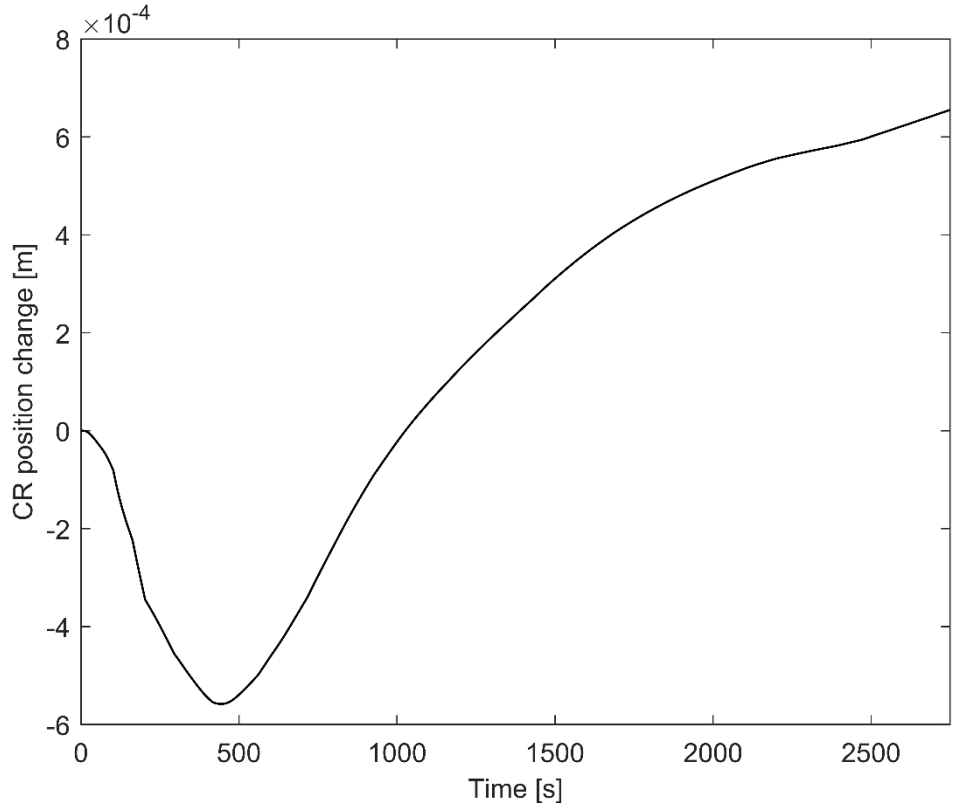

Fig. 15. CR position change during MOFC2 as predicted by TRACE code
(negative value corresponds to CRs withdrawal)

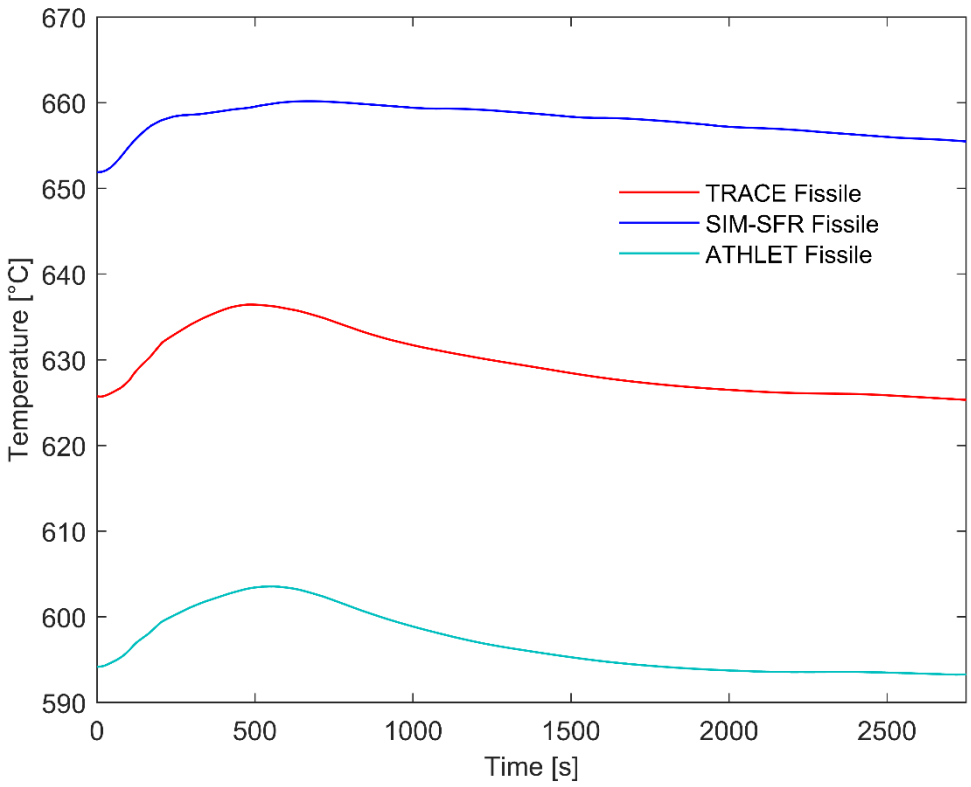

Fig. 16. Core-averaged fissile fuel temperature during MOFC2 transient

5.3. MOFC3: -10% primary mass flowrate reduction at 662 MWth

The MOFC3 transient is initiated at 662 MWth by decrease of the primary flow, which also results in subsequent drop of the core inlet temperature by about 8°C during the transient. Results of simulations with the three codes are depicted in Fig. 17-23. A specific power evolution shown in Fig. 17 results from reactivity contributions acting on different time scales. As the mass flow decreases during the first 75 s (see Table 22 in section 3.6.3) the core outlet temperature increases and corresponding heating up of the CRDL takes place along with CRs insertion, introducing a negative reactivity (see Fig. 18). Small positive reactivity contribution of sodium density and Doppler due to sodium heatup and fuel cooling down do not compensate the negative component in these first seconds of the transient. The imposed continuous decrease of the core inlet temperature (Fig. 21) drives introduction of a positive reactivity due to contraction of the diagrid plate and corresponding core compaction and contraction of the strongback, thus introducing enough reactivity to ensure a power rise up to 500 s of the transient. The core outlet temperature (Fig. 20) stabilises as a result of decreased inlet temperature and increased core heatup (Fig. 21 and Fig. 19),

what stabilises the positive contribution of the CRDL effect. After about 500 s of the transient, an insertion of the CRs (Fig. 22) and introduction of a strong negative reactivity (Fig. 18) is observed originating from vessel wall contraction and resulting in a power drop and stabilization at slightly more cooled conditions of the core.

Prediction of this transients by three codes exhibit particular challenges. As in MOFC2 case, the results of TRACE and ATHLET differ from SIM-SFR predictions. Both TRACE and ATHLET fail to reproduce accurately the expected experimental power and sodium heatup transient evolution. This may be attributed to challenges of reproducing the reactivity effects, acting on different time scales with opposite sign. Thus overall, both extremums of the power evolution were reproduced while the magnitude was reproduced poorly. The power stabilization seems to be reproduced accurately, implying that the vessel expansion components is treated reasonably. A reasonable agreement is observed for main reactivity contributions for these two solutions. This implies that resulting power evolution deviate from the expected experimental data due to 1) simplifications during modelling of structures thermal expansion, 2) lack of design details, and 3) accuracy of input data for this transient, extracted from the published materials. Somewhat better agreement was reported in [5] for analysis with TRACE code. The difference in the results lay in 1) different set of reactivity coefficients used in [5], e.g. the CR position effect is accounted for in a different way, 2) parameters of heat structures differ from proposed in the benchmark, 3) pin model of FRED was used (while a simplified approach is used in the benchmark with pre-specified fuel-gap conductance).

Results of SIM-SFR also differ from the experimental data. The power initial drop and final stabilisation are reproduced reasonably accurate, while the power peak is also smeared as compared to the experimental curve. Evolutions of core outlet, CRDL, strongback and vessel temperatures differ from the ones of TRACE and ATHLET noticeably, resulting in a different decomposition of the transient reactivity. The same way as for TRACE code, a better agreement for these transient conditions was reported in [5]. The main reason for the observed differences lays in a different set of reactivity coefficients used in this benchmark in comparison with those stated in [5]. For example, in case of SIM-SFR the diagrid expansion effect and sodium density reactivity effect values are more than 2 times less than the ones reported in [5]. Using a completely different set of reactivity coefficients in comparison with [5], results in a larger differences of simulation results when compared to the experimental data. It should be mentioned here as well, that two sets of reactivity coefficients were developed in [5] independently by PSI and KIT for TRACE and SIM-SFR, respectively as results of calibration, in order to reproduce the selected transients, while in this study the reactivity coefficients were calculated during the static neutronics phase of the benchmark and the selected parameters of the structure expansion models were calibrated using model

implemented in TRACE [6]. In SIM-SFR, some of the proposed new data for the benchmark could not be accounted for (i.e. constant fuel-clad gap conductance values, etc.) due to different modelling features, as already stated in Section 4.2.

The same level of fuel temperature discrepancies is kept for the MOFC3 as observed for MOFC1 and MOFC2 (Fig. 23).

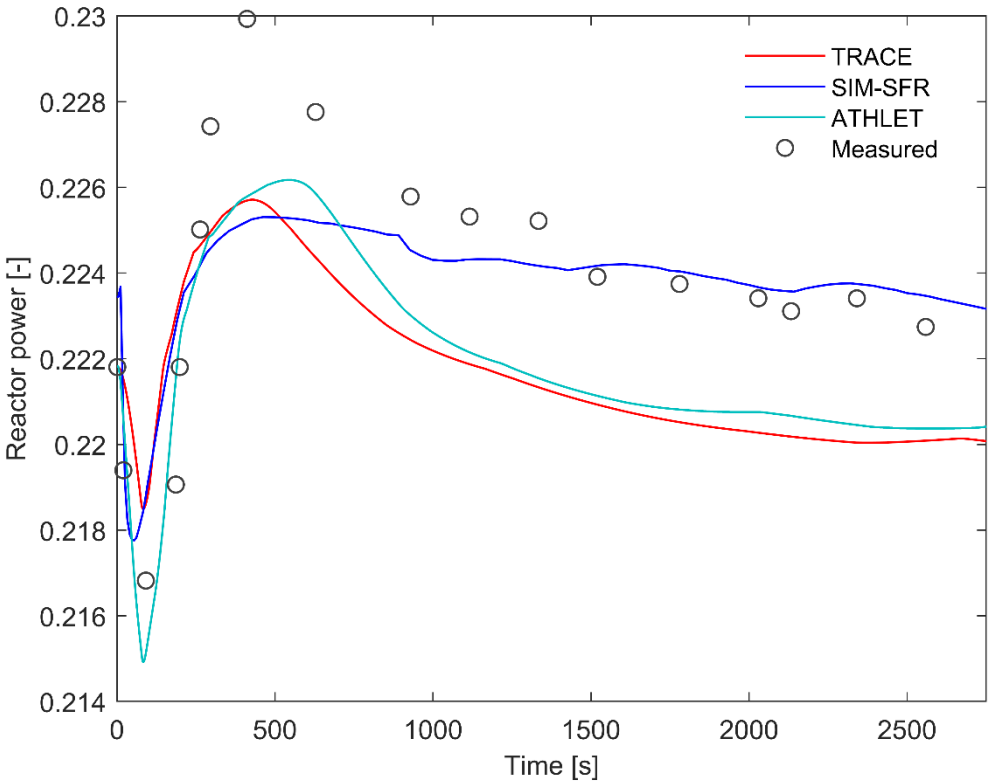

Fig. 17. Reactor power evolution in MOFC3 transient

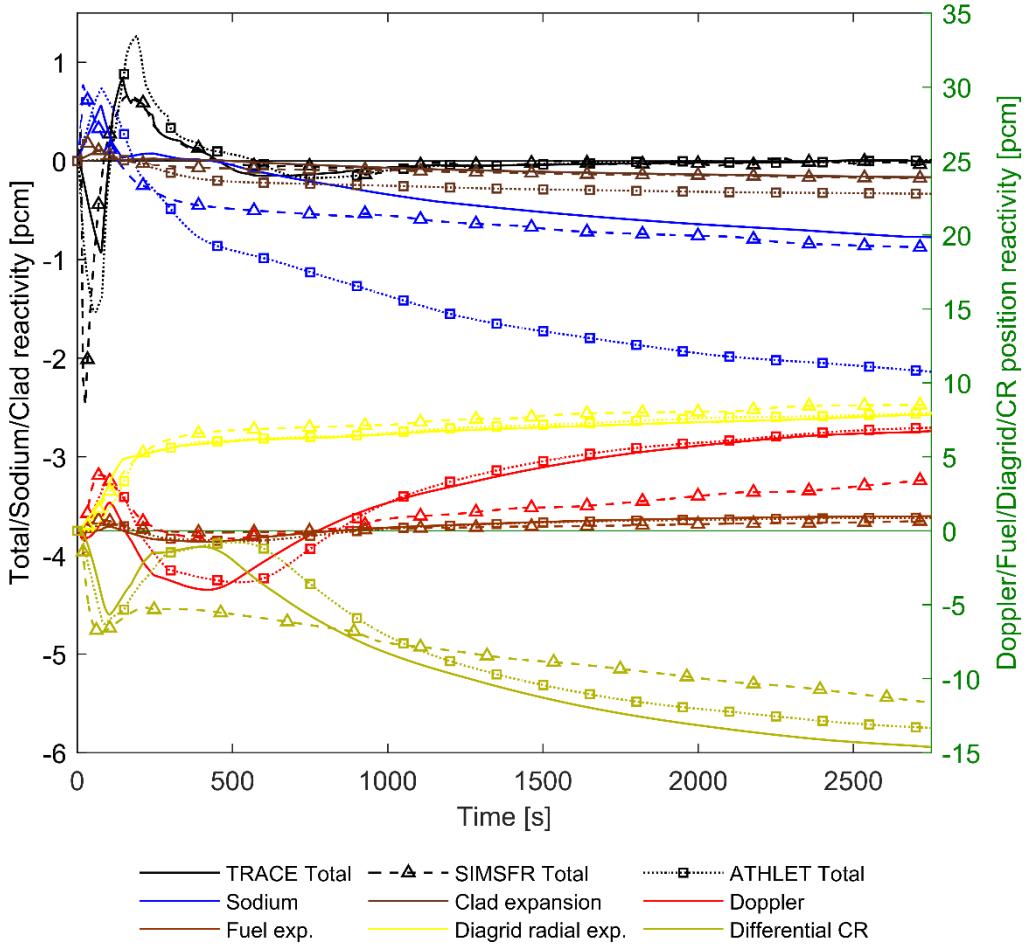

Fig. 18. Core reactivity and its decomposition during MOFC3 transient predicted by different codes (total, sodium density and clad expansion reactivity refer to Y-axis to the left; and Doppler, fuel axial expansion, diagrid radial expansion and CR position reactivity refer to Y-axis to the right)

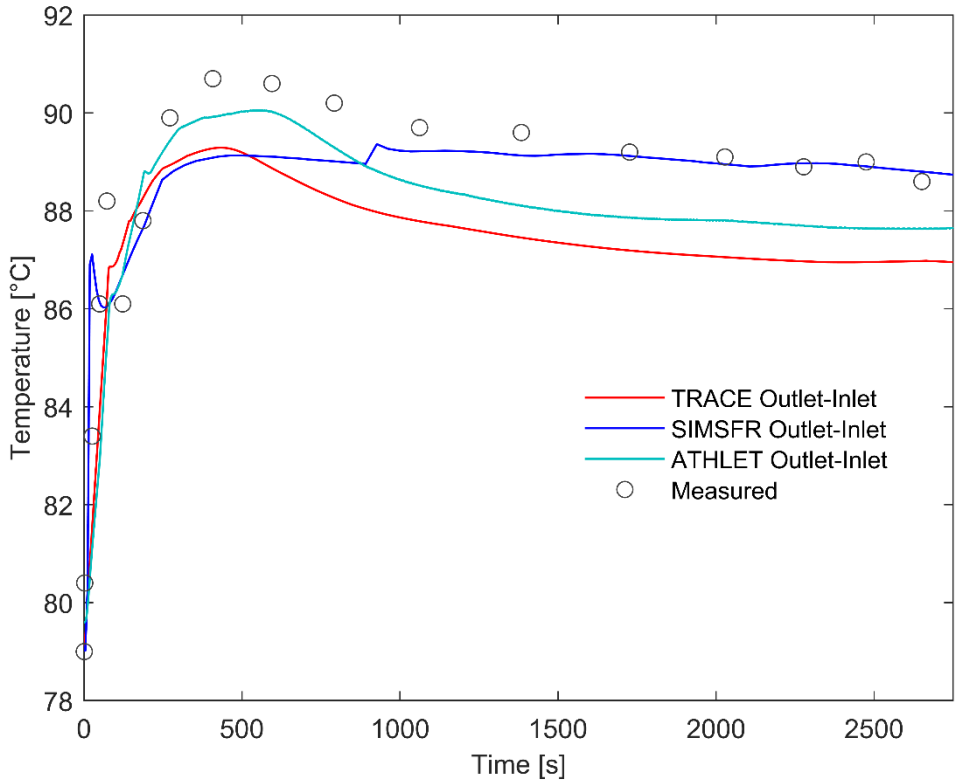

Fig. 19. Sodium core heatup in MOFC3 transient

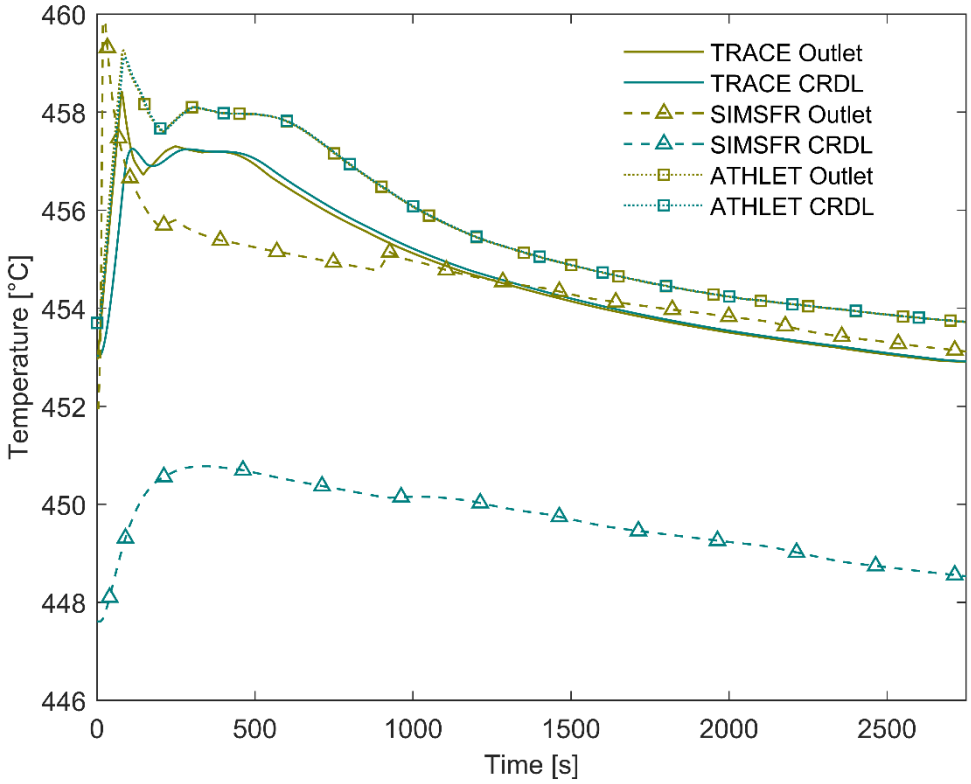

Fig. 20. Core outlet and CRDL temperatures during MOFC3

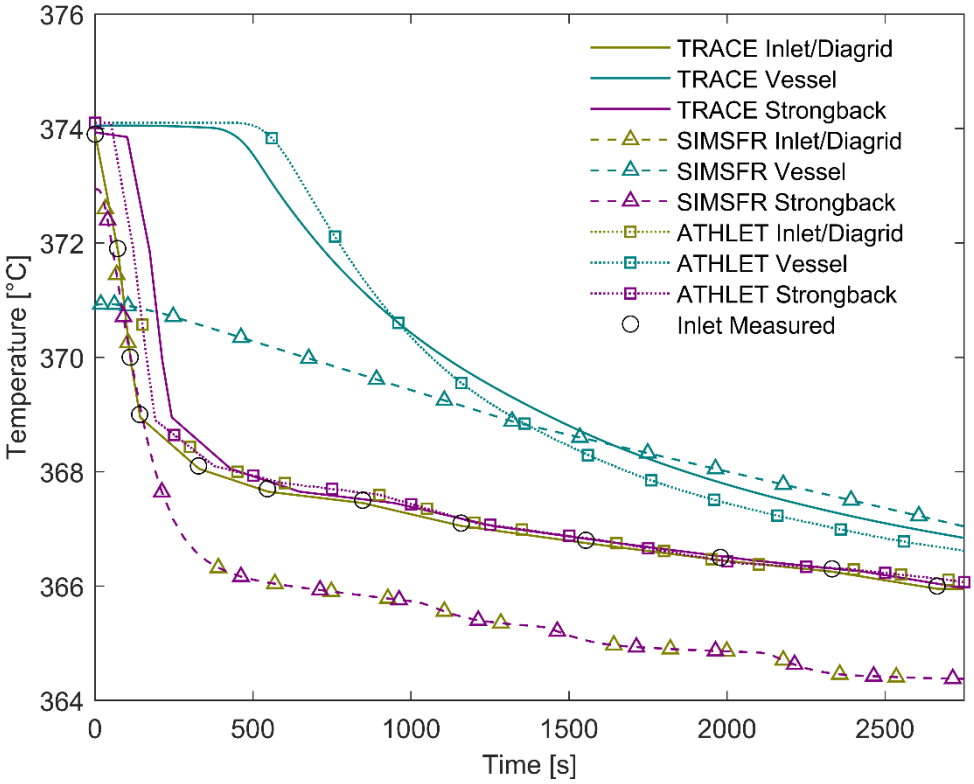

Fig. 21. Core inlet, diagrid plate, strongback, vessel temperatures during MOFC3 transient

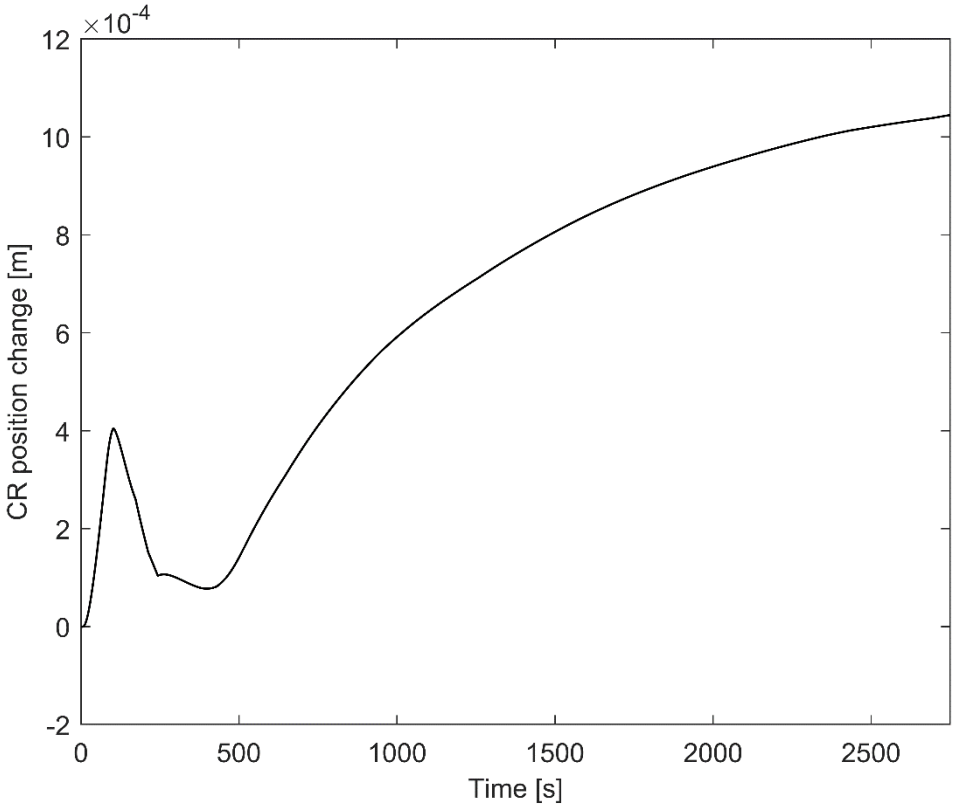

Fig. 22. CR position change during MOFC3 as predicted by TRACE code (negative value corresponds to CRs withdrawal)

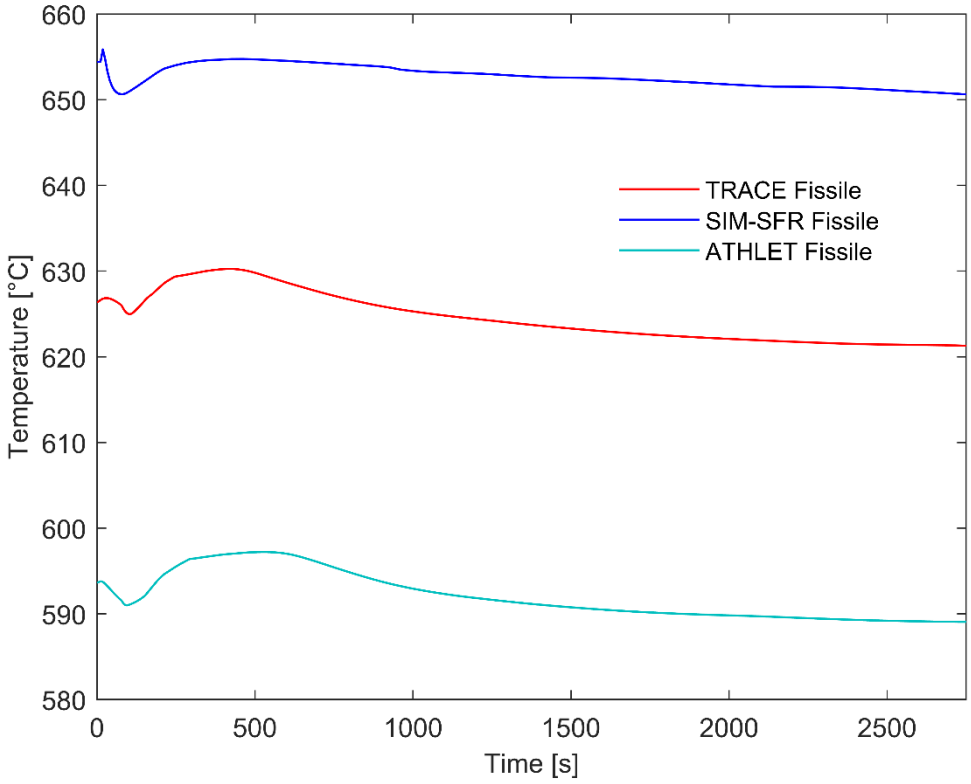

Fig. 23. Core-averaged fissile fuel temperature during MOFC3 transient

5.4. RS: -74 pcm stepwise reactivity insertion at 1542 MWth

The RS transient was initiated at the power level of 1542 MWth (around 50% nominal) by a step-wise insertion of a control rod with corresponding total reactivity of -74 pcm. The nature of this transient is similar to the one of MOFC1. Evolution of the selected parameters predicted by the three codes is given in Figs. 24-30. As noted in section 3.6.4, initial steady state conditions were perturbed by a decrease of core inlet temperature by ~1°C during the first ~300 s of the modelling prior to the reactivity insertion, resulting in a predicted power rise by about 8 MWth, which is also observed in the experimental data as plotted in Fig. 24.

An appropriate agreement can be stated for reactor power evolution predicted by the three codes. Only minor discrepancies are observed between the solutions and also with respect to the experimental data. Both initial power step-wise drop and subsequent power stabilisation are well reproduced by all models. Reactivity and its decomposition (Fig. 25) also demonstrate agreement between solutions. Following the step-wise reactivity insertion, a rapid Doppler and fuel expansion positive reactivity is introduced, accompanied by a reactivity due to the withdrawal of CR out of the core (Fig. 29), as a result of fuel pellet stack cooling down and contraction, and decrease of CRDL

temperature (Fig. 27). The total magnitude of these power drops is defined to a large extent by a balance between fuel-clad gap conductance and the Doppler Constant and to a minor extent by the CR position worth and fuel axial expansion effect. After the power drop, a slight increase is observed (up to *t*=1000 s in Fig. 24), originating from further withdrawal of CRs (see Fig. 29) as the decrease of the core inlet temperature by about 6°C (Fig. 28) introduces a positive reactivity due to diagrid and strongback cooling down. The wavy behaviour during power stabilization is also originating from the imposed wavy evolution of the core inlet sodium temperature, as can be visible in Fig. 28. Further power increase is mitigated by a strong negative reactivity due to vessel contraction as the CRs are being inserted into the core (see Fig. 29). Overall the predicted by TRACE code evolutions of the CRs position change parameter in RS and MOFC1 transients exhibit very similar qualitative behaviour (see Fig. 8 and 29).

It is worth to note that for the RS transient, both TRACE and SIM-SFR models used in the benchmark demonstrate coherency with the results, obtained in [5]. Thus differences between the reactivity coefficients sets and modelling features used here and in [5], have only a minor impact on the simulation results of this particular transient, thus the agreement to experimental data remains equally good.

With increase in reactor power as compared to MOFC1-MOFC3 transient scenarios, the differences between the codes in prediction of fuel temperature increased as depicted in Fig. 30.

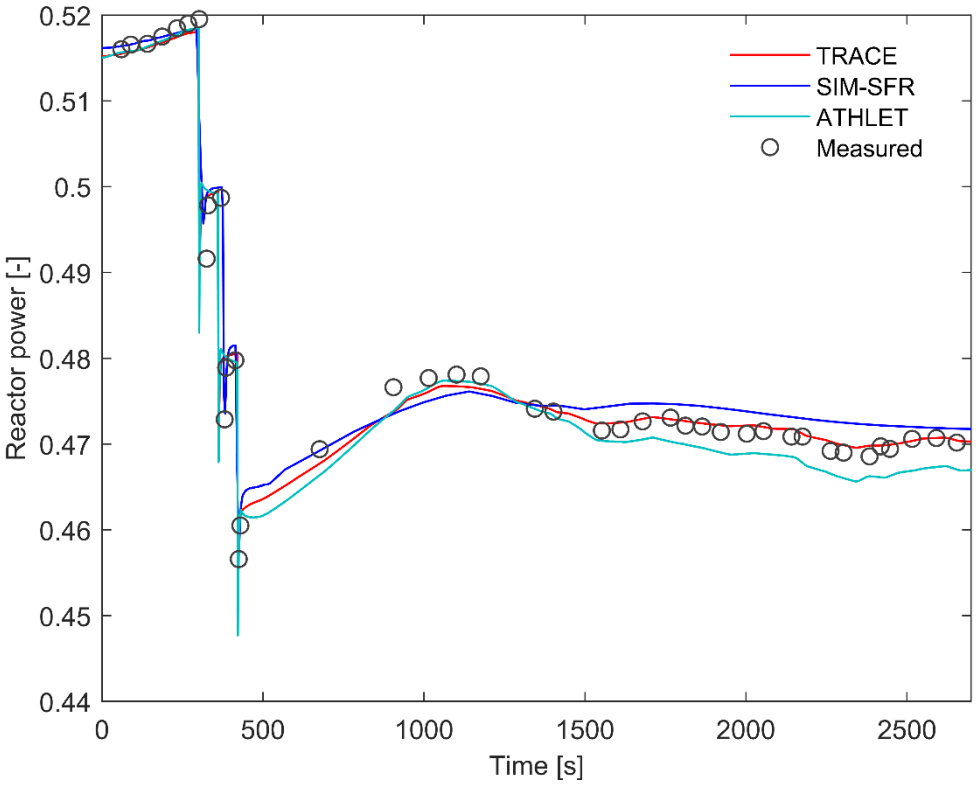

Fig. 24. Reactor power evolution in RS transient

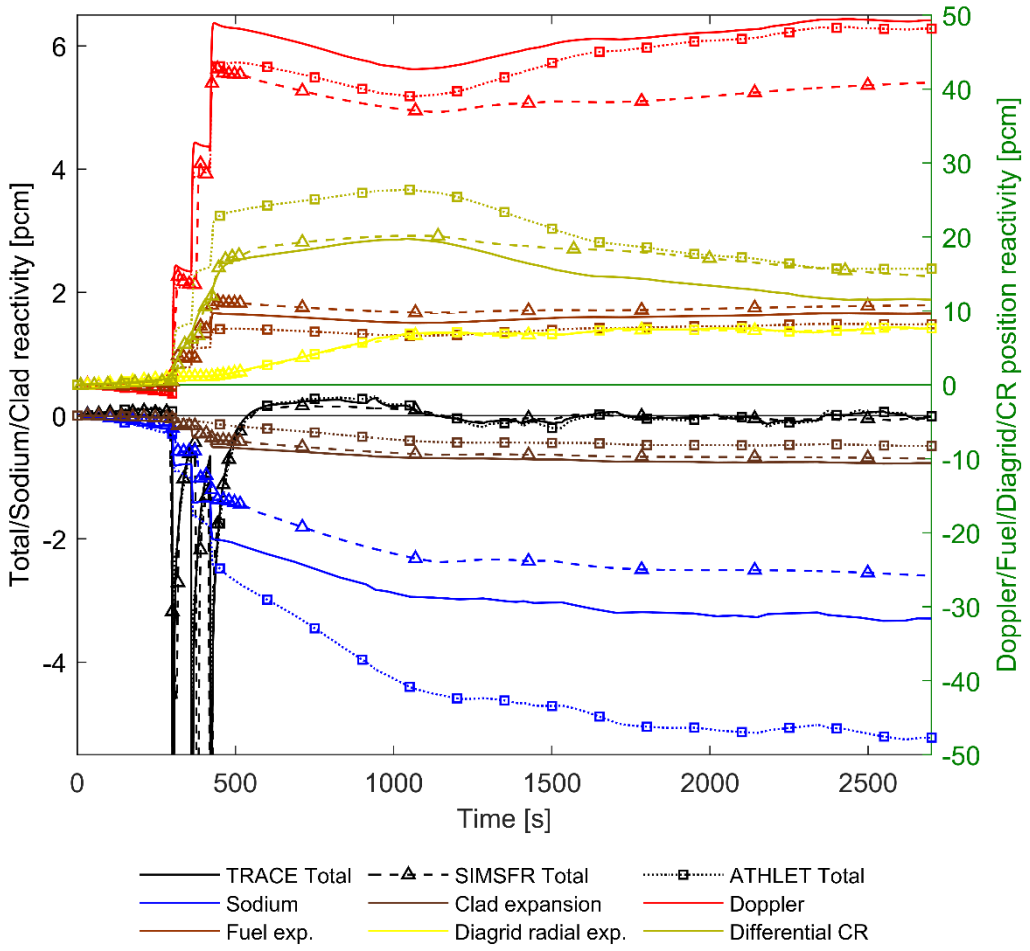

Fig. 25. Core reactivity and its decomposition during RS transient predicted by different codes (total, sodium density and clad expansion reactivity refer to Y-axis to the left; and Doppler, fuel axial expansion, diagrid radial expansion and CR position reactivity refer to Y-axis to the right)

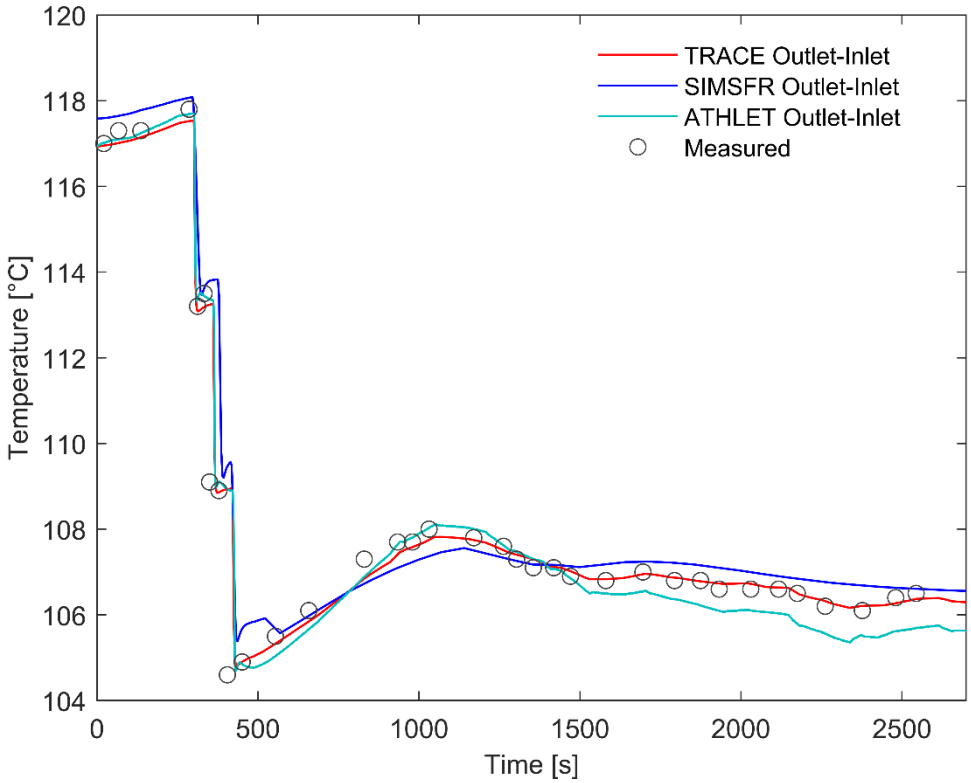

Fig. 26. Sodium core heatup in RS transient

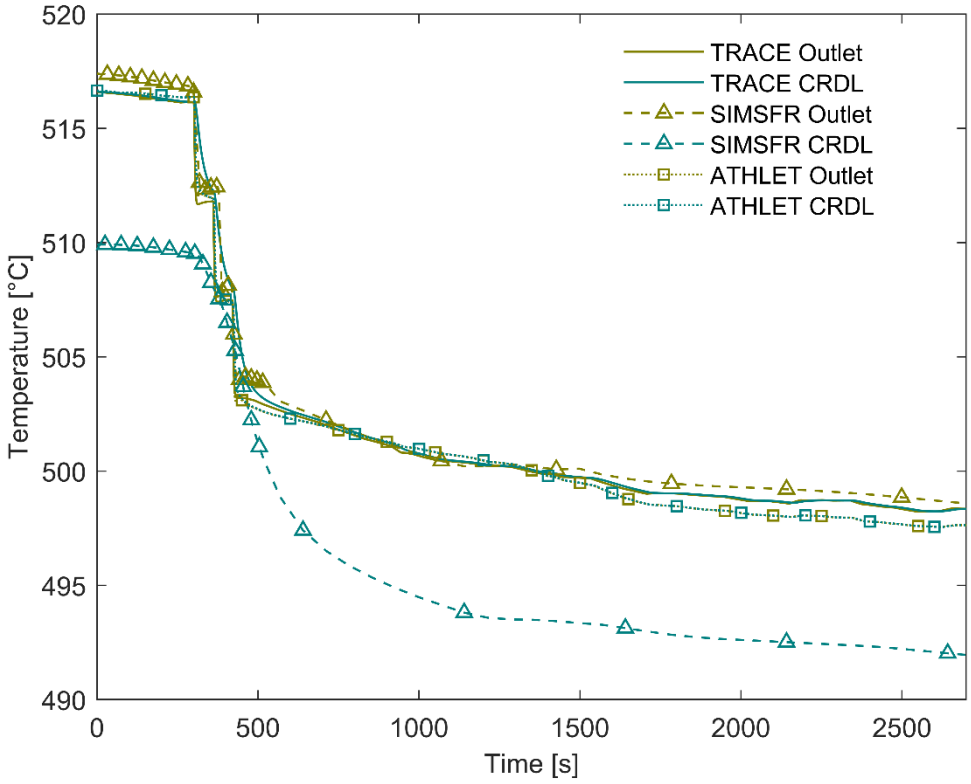

Fig. 27. Core outlet and CRDL temperatures during RS

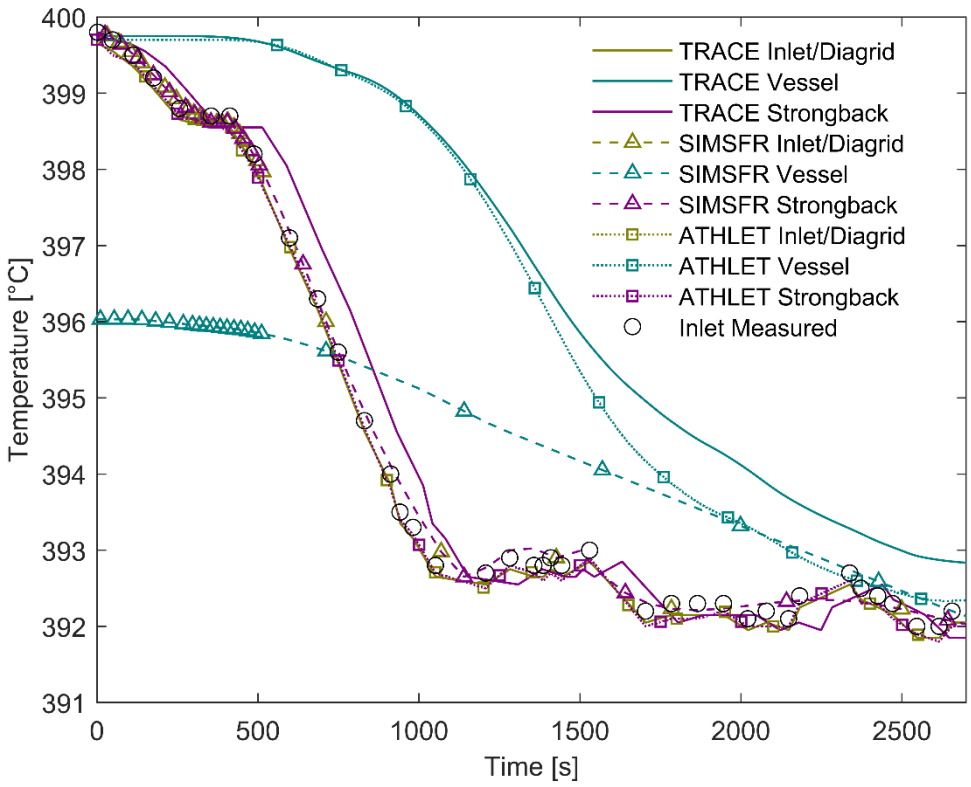

Fig. 28. Core inlet, diagrid plate, strongback, vessel temperatures during RS transient

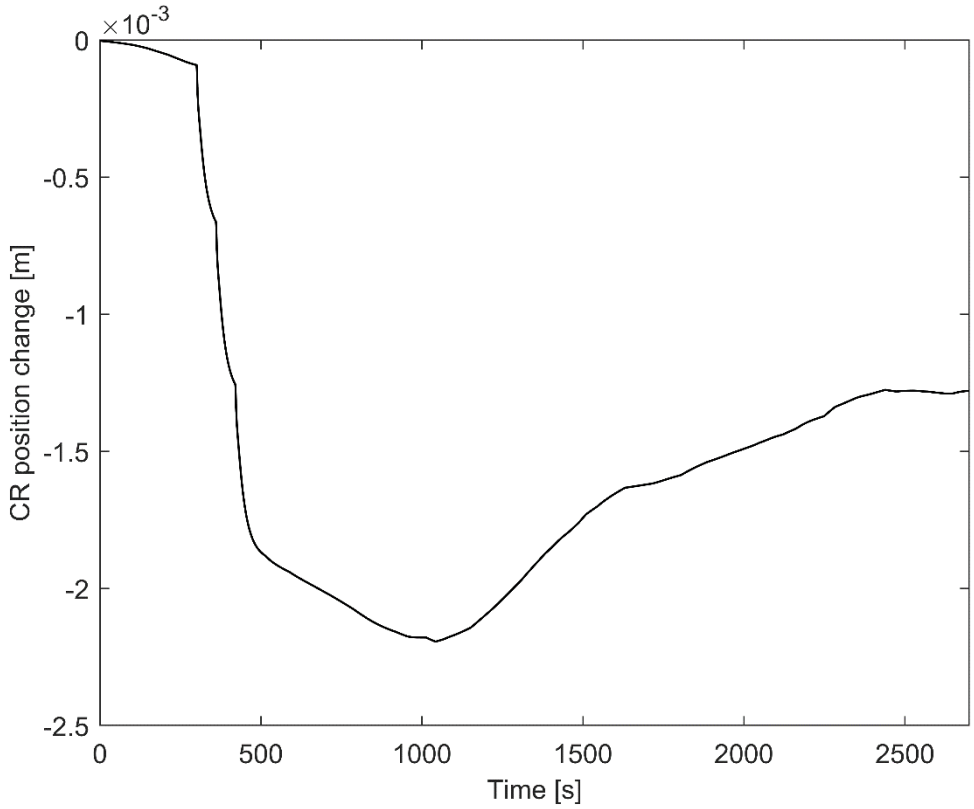

Fig. 29. CR position change during RS as predicted by TRACE code

(negative value corresponds to CRs withdrawal)

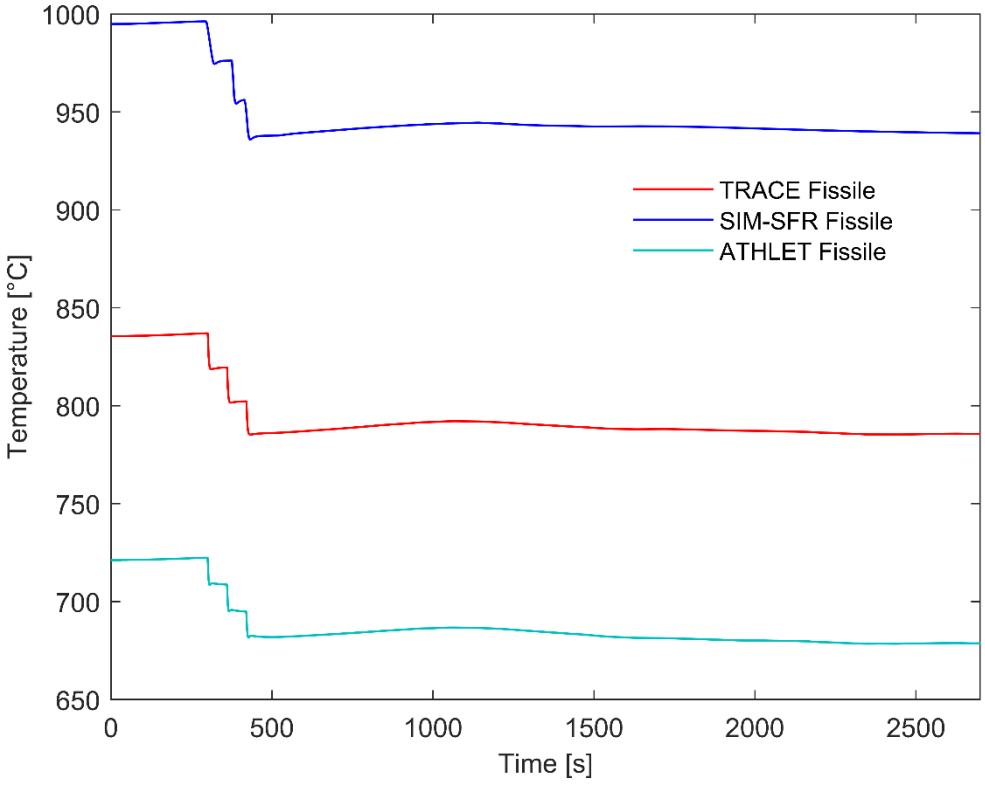

Fig. 30. Core-averaged fissile fuel temperature during RS transient

5.5. PFS: -10% primary mass flowrate reduction at 1415 MWth

The PFS transient initiated at ~50% nominal power is naturally similar to MOFC3, discussed in Chapter 5.3. Reduction of primary mass flow by 11.5% was introduced after the reactor was stabilised at 1415 MWth, while the variation of core inlet temperature due to the subsequent response of the secondary system is imposed as a boundary condition. Evolution of selected parameters as predicted by the three codes is given in Figs. 31-37.

The initial perturbation of the mass flow rate results first in an insertion of negative reactivity (Fig. 32) and a power drop (Fig. 31) originating from the insertion of CRs (Fig. 36). This insertion accounts for elongation of CRDL, as the core outlet and CRDL temperatures increases by about 10°C (Fig.34). The rapid mass flow drop and sodium heatup increase (Fig. 33) result in an insertion of a small positive Doppler reactivity due to fuel heatup, followed by a fuel cooling down due to the drop of the power level. This positive contribution together with the rising contributions of diagrid and strongback, originating from their cooling down, drive the power rise during first ~400 s of the transient (Fig. 31). This is followed by power ramp and stabilization with kind of wavy behaviour, which occurs as the positive reactivity is compensated by a strong negative reactivity related to the vessel cooling down (Fig. 32).

Power and sodium heatup evolution fits reasonably to the experimental data, as depicted in Figs. 31 and 33. There is a close agreement between TRACE and ATHLET results on power evolution for the first 700 s of the transient. The evolution follows the experimental data with a slight shift down, thus failing to reproduce the magnitude of both inflections of the power trace. After 700 s, ATHLET power deviates stronger from the experimental and TRACE data, due to a stronger reactivity contribution of CRs position (Fig. 32). The reason of this is a slightly stronger negative component of the vessel as compared to TRACE, as in accord with the vessel temperature evolution in Fig. 35. This effect was not that pronounced in the MOFC3 transient because of a smaller total variation of the core inlet temperature, and correspondingly of the vessel one.

SIM-SFR predicts a smaller power peak while the power stabilizes at the level, prescribed by the experimental data. The reactivity decomposition is very similar to the one of TRACE code in this transient. The same level of discrepancies is observed for prediction of temperatures of CRDL, vessel and strongback as compared to TRACE and ATHLET. As already mentioned in Chapter 5.3, the main reason for the observed differences for SIM-SFR lays in a different set of reactivity coefficients used in this benchmark, in comparison with those stated in [5]. Similar discrepancies are observed for the fuel temperature, as depicted in Fig. 37.

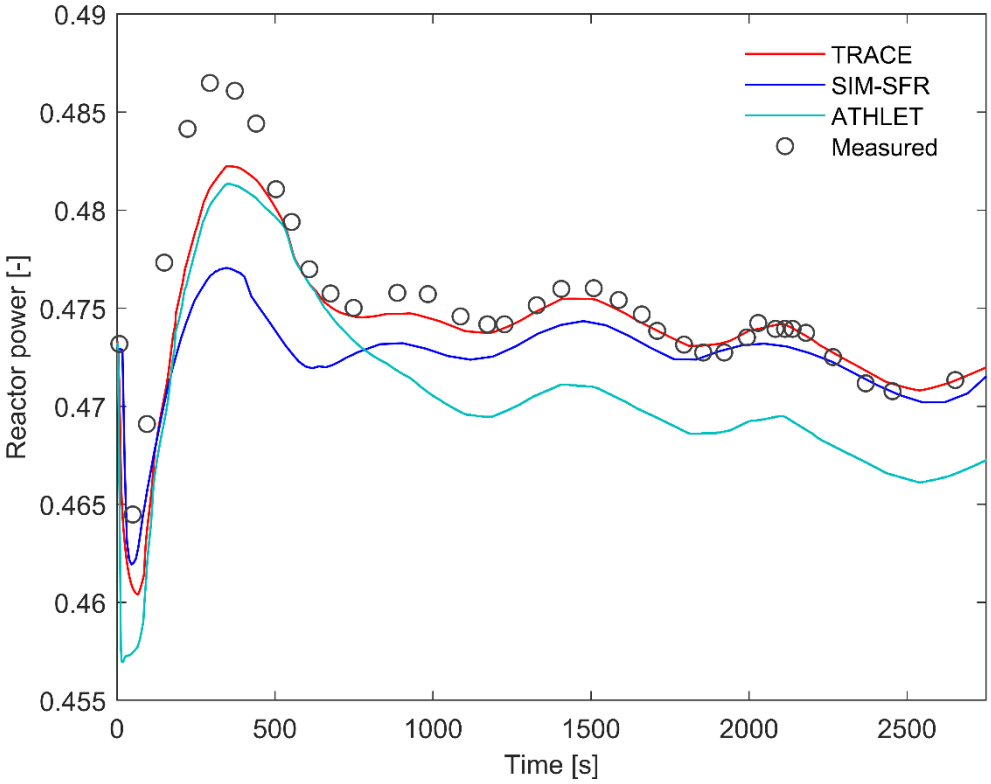

Fig. 31. Reactor power evolution in PFS transient

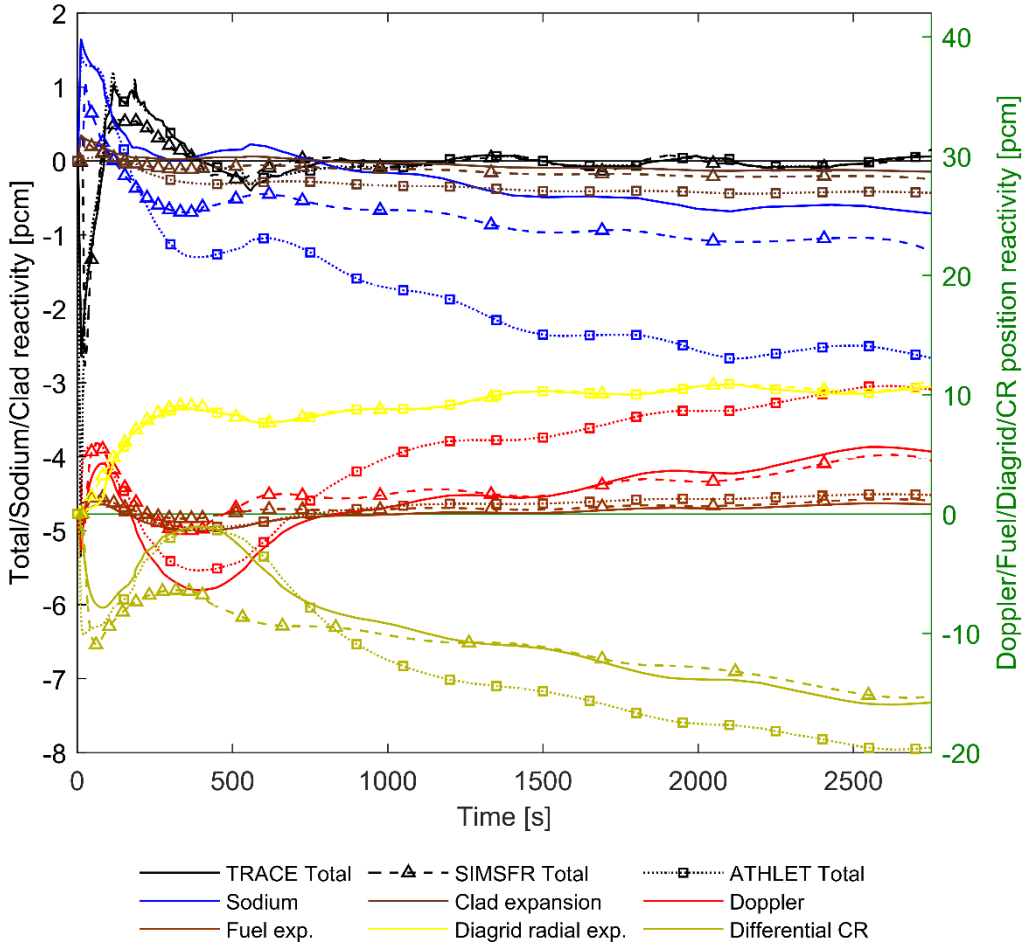

Fig. 32. Core reactivity and its decomposition during PFS transient predicted by different codes (total, sodium density and clad expansion reactivity refer to Y-axis to the left; and Doppler, fuel axial expansion, diagrid radial expansion and CR position reactivity refer to Y-axis to the right)

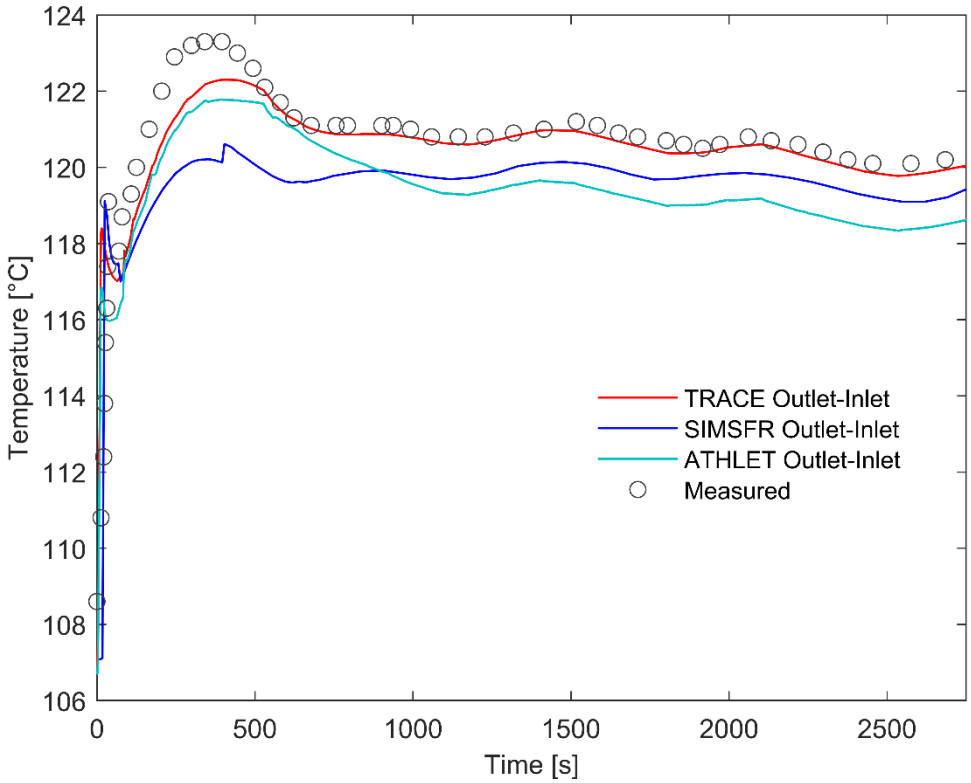

Fig. 33. Sodium core heatup in PFS transient

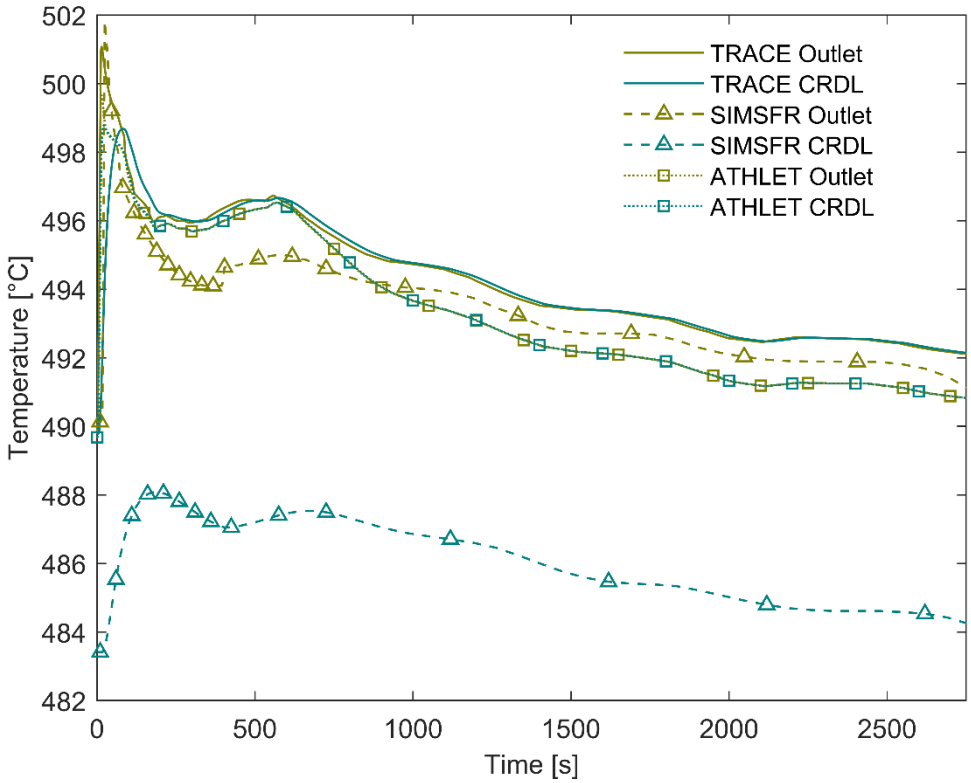

Fig. 34. Core outlet and CRDL temperatures during PFS

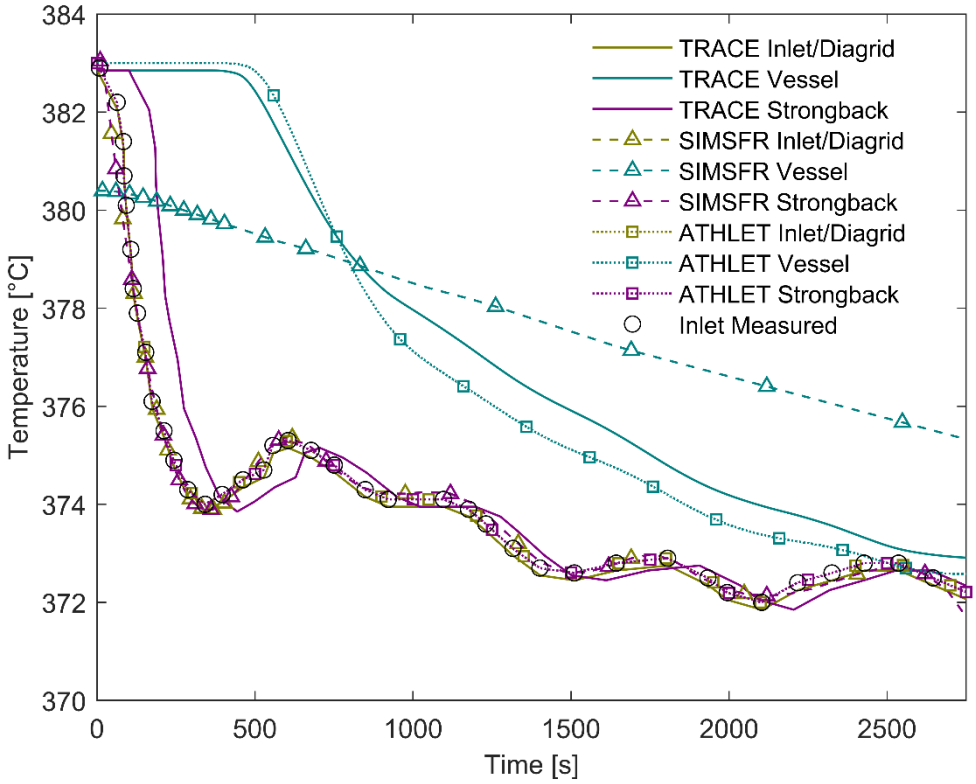

Fig. 35. Core inlet, diagrid plate, strongback, vessel temperatures during PFS transient

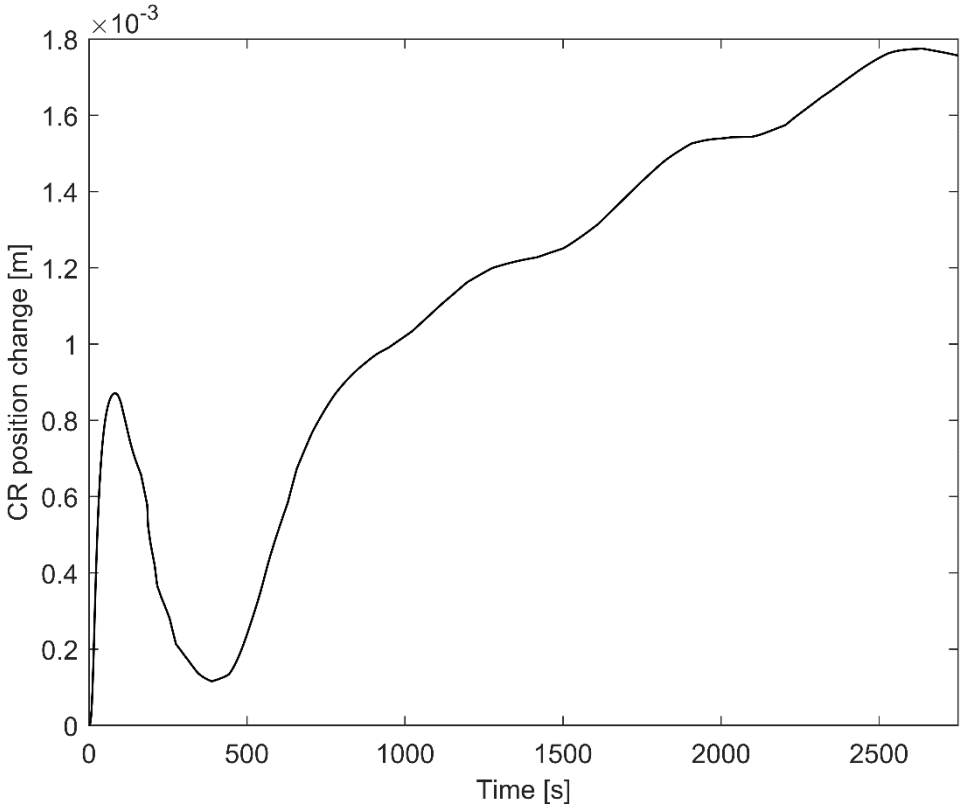

Fig. 36. CR position change during PFS as predicted by TRACE code

(negative value corresponds to CRs withdrawal)

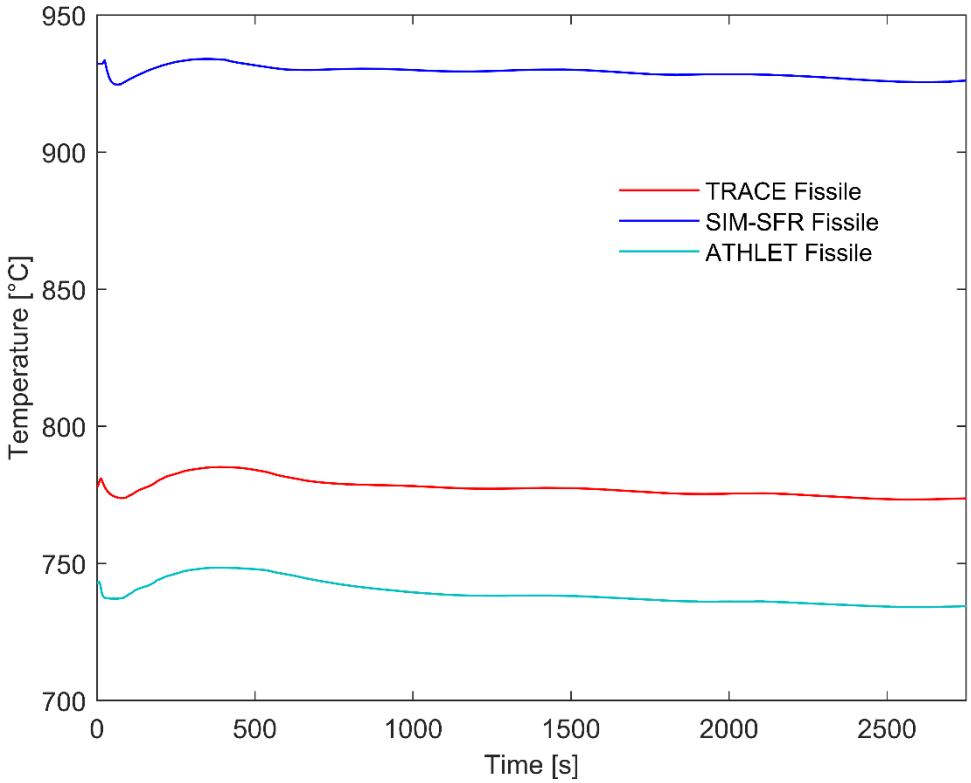

Fig. 37. Core-averaged fissile fuel temperature during PFS transient

5.6. SST: +30 pcm reactivity insertion at hot zero power

The self-stabilization test was performed analyzing a reactor response to a CR withdrawal at zero power conditions. As a steady state of the primary system was achieved at 179°C isothermal conditions keeping the reactor critical at nearly zero power, the insertion of 30 pcm positive reactivity was introduced. As it is noted in [5], modelling of this transient is essentially challenging and requires a high fidelity, dynamic fuel pin model as the feedback reactivities are initially solely due to the Doppler (fuel temperature increase), later followed by the expansion feedbacks. Evolution of selected parameters predicted by the three codes within the benchmark study is given in Figs. 38-45.

All codes predict the power rise followed by a stabilization ramp, as depicted in Fig. 38. Initial response of Doppler effect mitigates the initial power jump. The predicted fuel temperature (Fig. 44) and sodium heatup (Fig. 40) evolutions are in a reasonable agreement for all the codes. Additional negative reactivity of CRs position is introduced as CRDLs are elongating, due to an increase of the core outlet temperature, and fuel is expanding axially (first 1000 s). In the simplified approach of the benchmark (no dynamic pin heat transfer modelling), the peak power is defined to a large extent by two parameters of the model: the fuel Doppler Constant and the fuel-clad gap conductance. Thus the selected values allow a reasonable reproduction of this power peak. The primary and secondary

systems feedback results in a delayed start of increase of the core inlet temperature, as can be seen in Fig. 42. At this moment the structure expansion related feedbacks of first diagrid and later strongback are becoming visible, resulting in a negative reactivity insertion and a power ramp. In the latter phase of the transient (after ~1800 s of transient) the feedbacks are accompanied by a feedback of the vessel expansion and the corresponding withdrawal of CRs (Fig. 43). Overall, results of modelling of this particular transient demonstrate clear coherency with those reported in [5], implying appropriate choice of modelling assumptions and parameters even with a simplified approach on pin heat transfer.

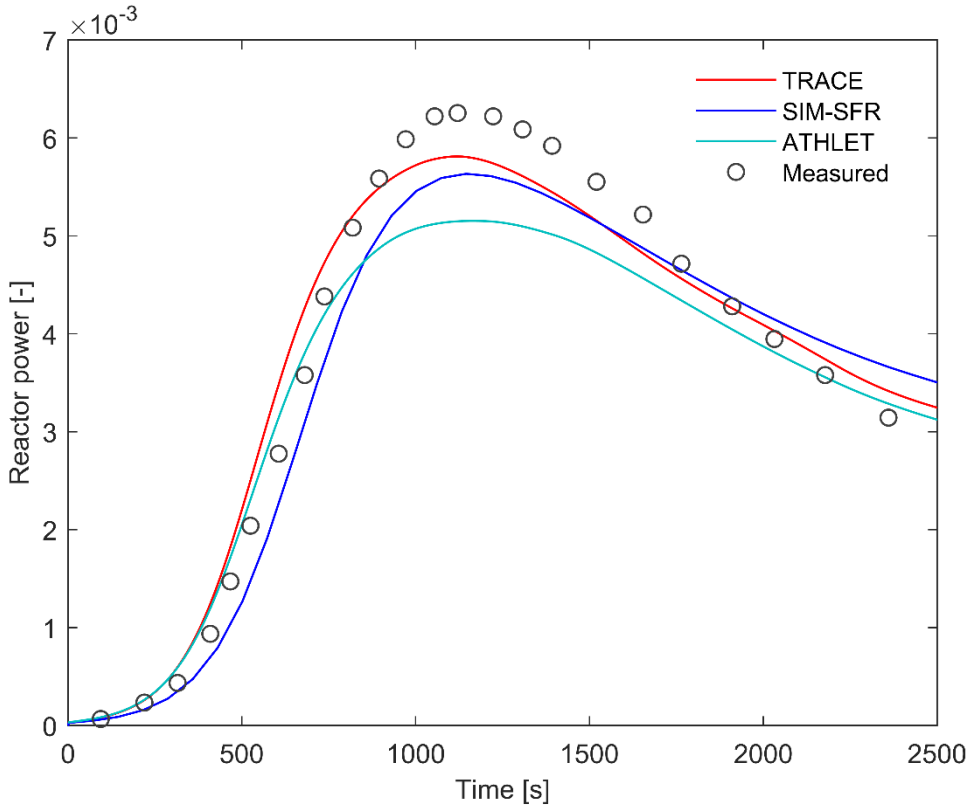

Fig. 38. Reactor power evolution in SST transient

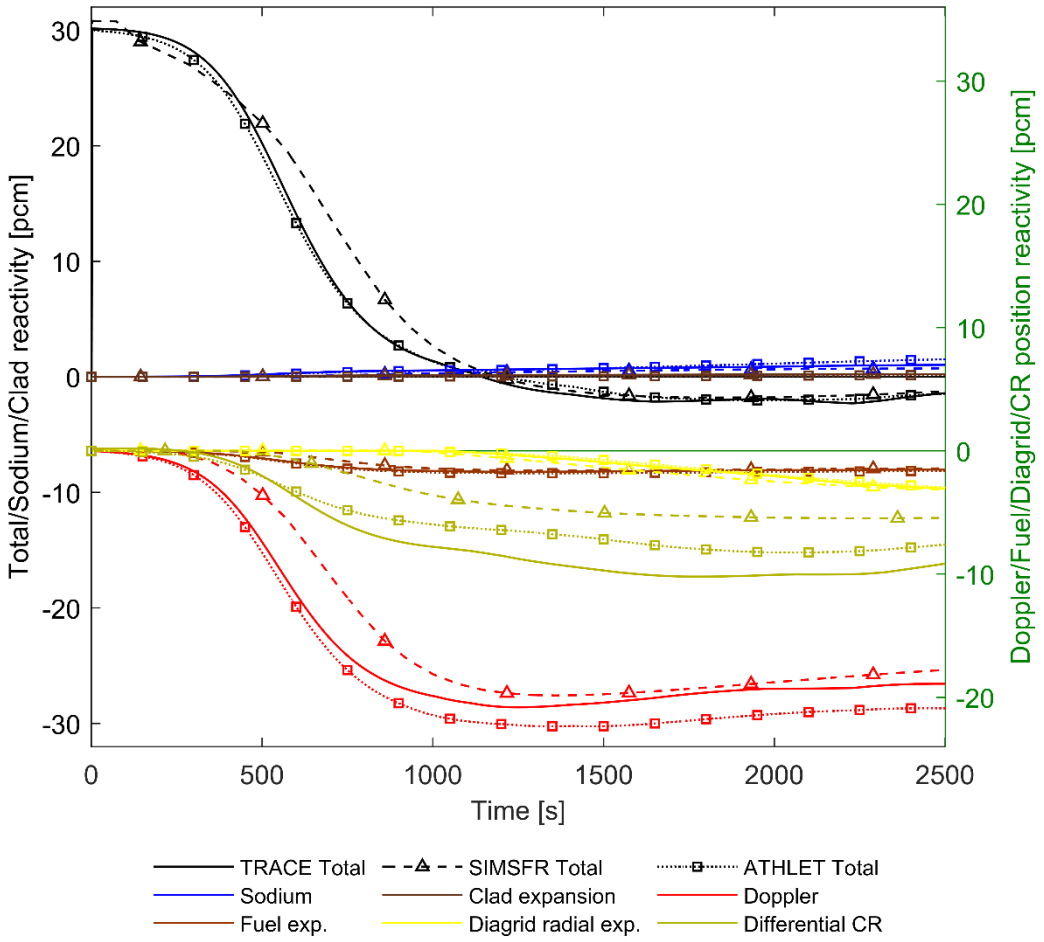

Fig. 39. Core reactivity and its decomposition during SST transient predicted by different codes (total, sodium density and clad expansion reactivity refer to Y-axis to the left; and Doppler, fuel axial expansion, diagrid radial expansion and CR position reactivity refer to Y-axis to the right)

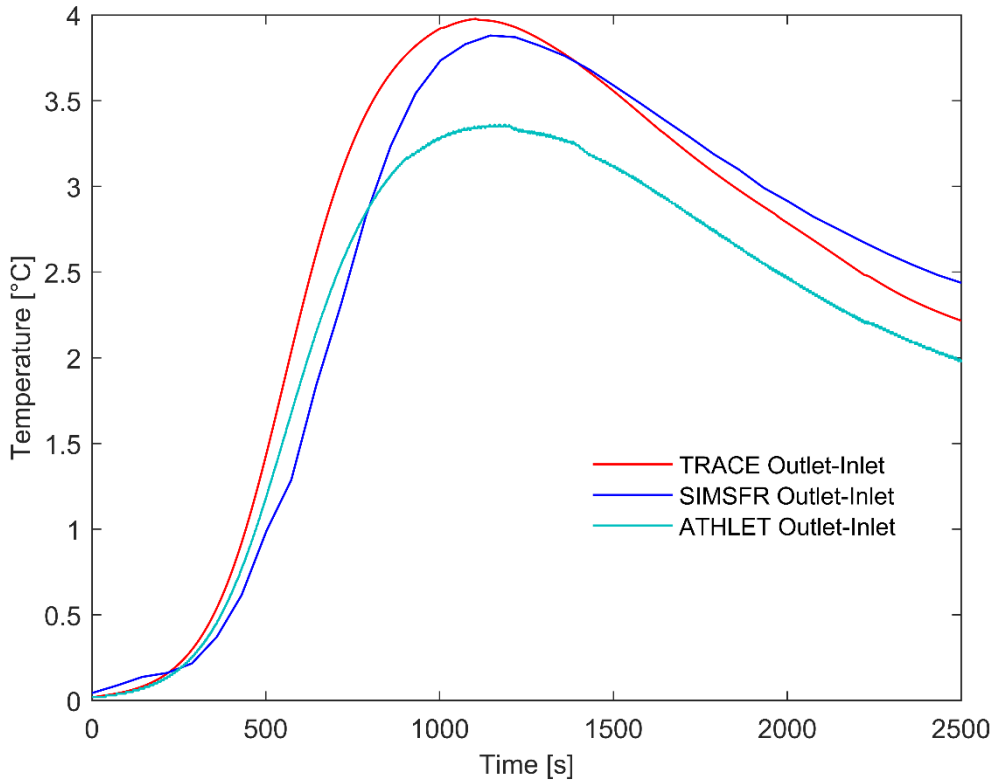

Fig. 40. Sodium core heatup in SST transient

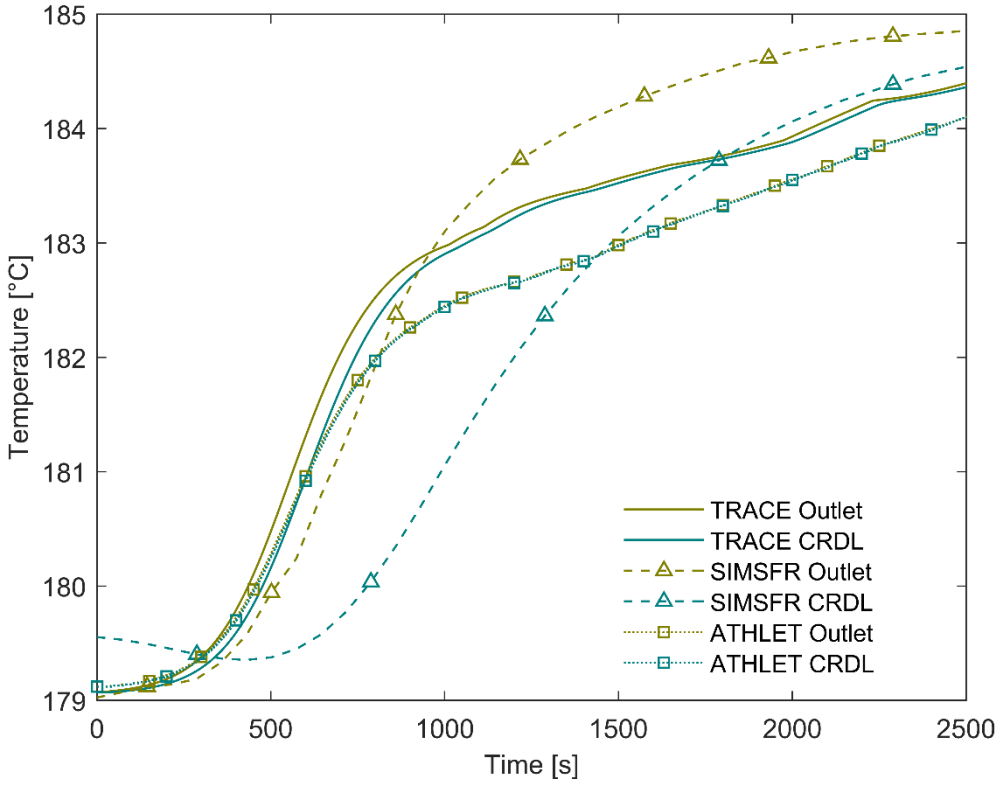

Fig. 41. Core outlet and CRDL temperatures during SST

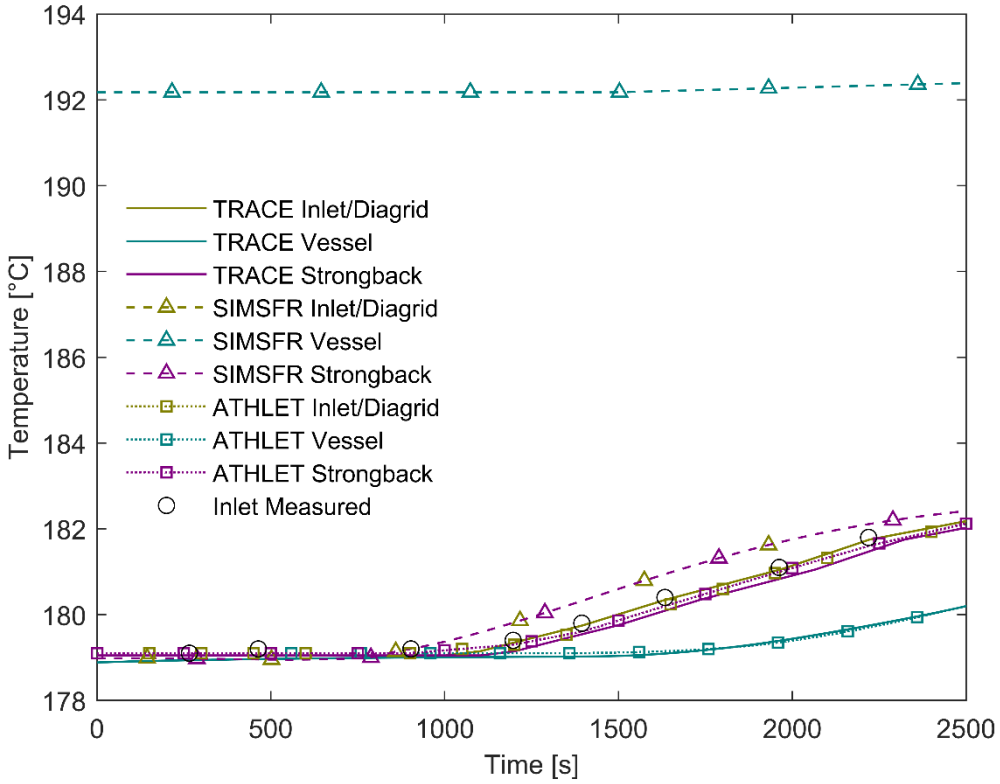

Fig. 42. Core inlet, diagrid plate, strongback, vessel temperatures during SST transient

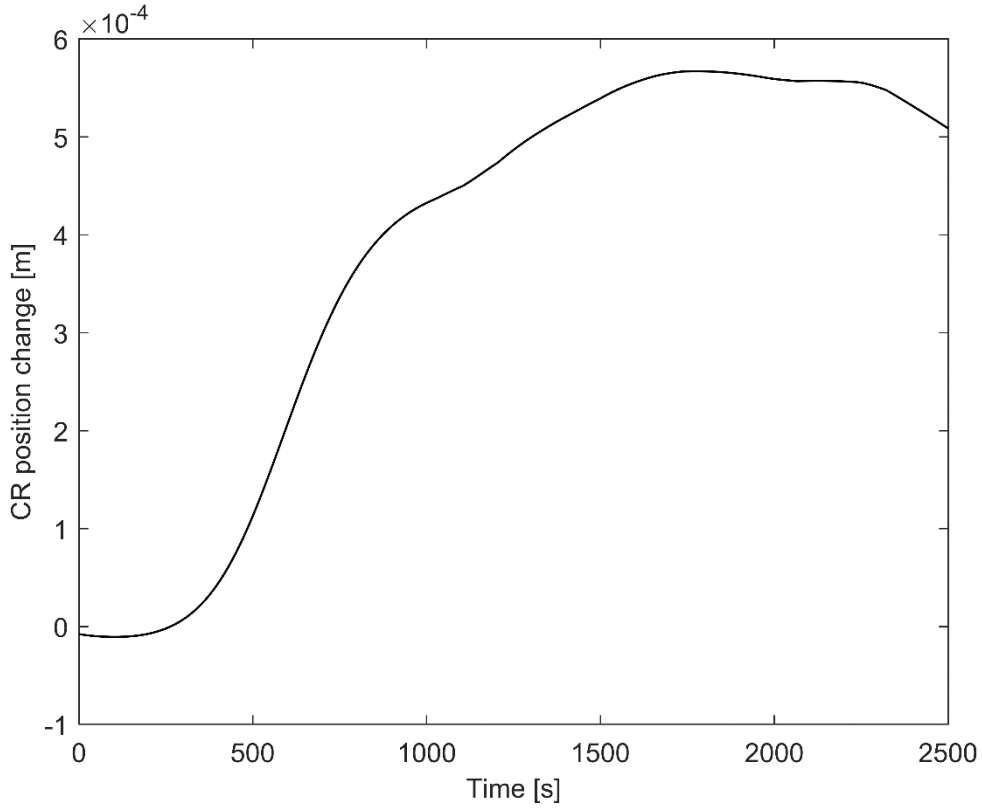

Fig. 43. CR position change during SST as predicted by TRACE code
(negative value corresponds to CRs withdrawal)

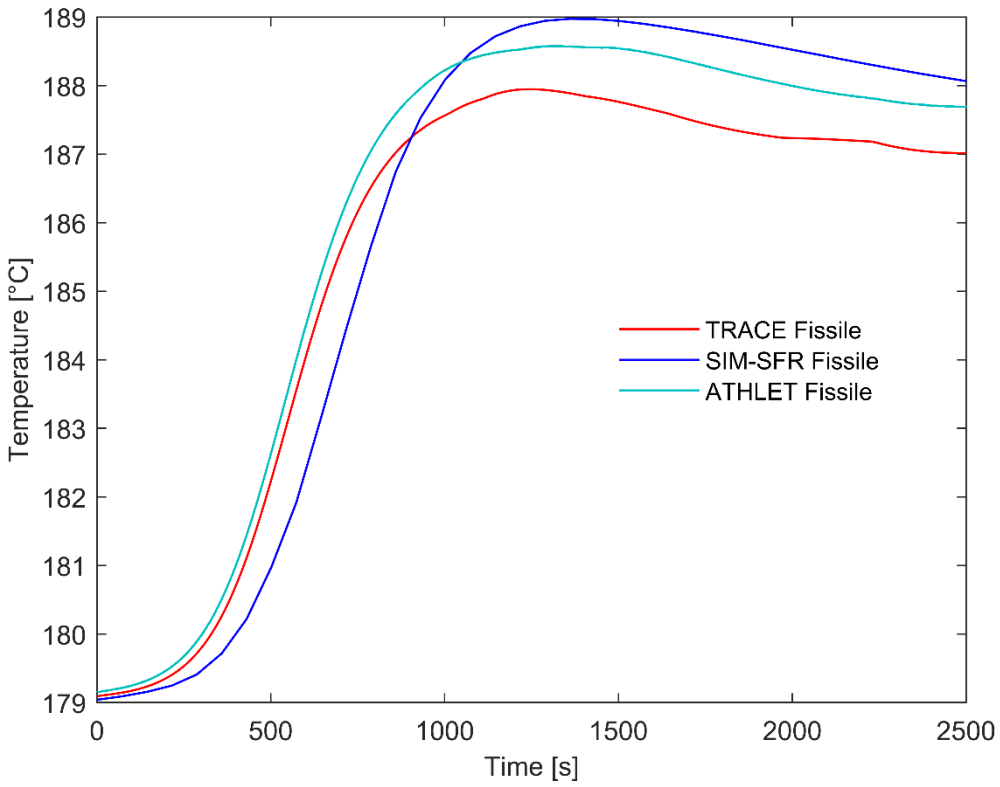

Fig. 44. Core-averaged fissile fuel temperature during SST transient

7. CONCLUSIONS

The paper summarizes results of the second phase of the SPX benchmark related to modelling of the core transient behaviour.

The first part of the paper presents the transient benchmark specification in two data sets: 1) description of the simplified SPX core model including recommendations for core nodalization and data for the point reactor kinetics modelling obtained at the first (static) phase of the benchmark; 2) data measured during six operational transient experiments performed in the frame of the start-up tests in terms of initial core conditions and time histories of a number of measured parameters derived from the open literature sources. Peculiarity of this part of the benchmark exercise lays in 1) the necessity of the modelling of thermal expansion of in-reactor structures (diagrid plate, strongback, control rods drive lines, reactor vessel) and related reactivity feedbacks, and 2) proposed simplified assumptions for number of uncertain parameters and characteristics of the modelled core, such as fuel-clad gap conductance values, control rods position, physical parameters

of the modelled structures. These parameters were first assumed based on a reasonable engineering judgement and then calibrated in order to better represent the transient behaviour of the core, as compared to the available transient experimental data for all six cases.

The second part of the paper presents the calculational results of the transient benchmark obtained with three system codes: TRACE, SIM-SFR and ATHLET. For every transient the basic phenomenology and the nature of the modelled in-reactor structure expansion related feedbacks are discussed. A reasonable agreement between all solutions was obtained. With the proposed simplified model of the SPX core, it was possible to reproduce reasonably well a wide range of the experimentally observed transient conditions. Thus the paper can be of interest for the code developers working on coupled neutronic and thermal-hydraulic modelling of the liquid-metal fast reactors. Such models could be validated using the detailed specification of the transient benchmark for the large SFR core based on the experimental reactor data, and available few reference solutions especially in terms of the reactivity components important for better understanding of the underlying physics.

The analysis of the remaining discrepancies between the codes shows possible directions of the transient benchmark improvements, e.g.: 1) improvement of the quality of the core specification, including validated reactivity coefficients, positions of control rods for different power levels considered and other core data; 2) improvement of the quality of the measured data currently retrieved from open publication by digitizing the figures from these publications. A number of modelling features that can be important for better prediction of the transients were identified, e.g.: 1) the application of a high fidelity dynamic fuel pin heat transfer model, e.g. accounting for fresh fuel relocation, dynamic fuel-clad gap behaviour, etc.; 2) the application of more comprehensive models for the in-reactor structures, e.g. an accurate modelling of the whole primary system with its structures and cooling paths.

FUNDING

The work has been prepared within EU Project ESFR-SMART, which has received funding from the EURATOM Research and Training Programme 2014-2018 under the Grant Agreement No. 754501.

REFERENCES

1. A. Ponomarev, A. Bednarova and K. Mikityuk, "New sodium fast reactor neutronics benchmark", in Proceeding of PHYSOR 2018: Reactor Physics Paving The Way Towards More Efficient Systems, Cancun, Mexico, 2018.

2. K. Mikityuk et al., “ESFR-SMART: new Horizon-2020 project on SFR safety,” in IAEA FR2017, 2017.
3. A.Ponomarev, ”SPX Benchmark Part I: Static neutronics results”, NERS 2021 Special Issue
4. M. Vanier, P. Bergeonneau, J. C. Gauthier, M. Jacob, J. De Antoni, E. Gesi, P. Peerani and J. P. Adam, “Superphenix Reactivity Feedback And Coefficients”, Nuclear Science and Engineering, 106, pp. 30-36 (1990).
5. K. Mikityuk and M. Schikorr, “New Transient Analysis of the Superphenix start-up Tests”, Proceedings of International Conference on Fast Reactors and Related Fuel Cycles: Safe Technologies and Sustainable Scenarios (FR’13), Paris, France, March 4-7, 2013.
6. A. Ponomarev, K. Mikiytuk, “Modelling of Reactivity Effects and Transient Behaviour of Large Sodium Fast reactor”, ASME 2020.
7. J. Gourdon, B. Mesnage, J. L. Voitellier, M. Suescun, ”An Overview of Superphenix Commissioning Tests”, Nuclear Science and Engineering, Volume 106, Number 1, September 1990, Pages 1-10.
8. Ph. Bergeonneau, M. Vanier, M. Favet, J. De Antoni, K. Essig and J. P. Adam, ”An Analysis of the Dynamic Behavior of the Core”, Nuclear Science and Engineering, 106, pp. 18-29 (1990).
9. Ponomarev, A., Mikityuk, K., ”Analysis of hypothetical Unprotected Loss Of Flow in Superphenix start-up core: sensitivity to modeling details”. The proceedings of ICONE27: Vol. 2019.27. (pp. ICONE27-2050 (6 pp.). The Japan Society of Mechanical Engineers.
10. G. Flamenbaum, R. de Wouters, A. Le Bourhis, T. Newton and G. Vambenepe, “Superphenix Core-Loading Strategy Using the Checkerboard Pattern,” Nuclear Science and Engineering, 106, pp. 11-17 (1990).
11. Mikityuk, K., et al., “FAST: An advanced code system for fast reactor transient analysis”, Annals of Nuclear Energy, vol. 32, pp. 1613-1631, 2005.
12. Mikityuk, K., Krepel, J., Pelloni, S., Girardin, G., Chenu, A., Sun, K., Alonso, M., Marinoni, A., Adams, R., Reiterer, F., Monti, S. (Ed.). (2015). Fast Code System: Review of Recent Applications. International Atomic Energy Agency (IAEA): IAEA.
13. Schikorr, W. M., 2001. Assessment of the kinetic and dynamic transient behavior of sub-critical systems (ADS) in comparison to critical reactor systems. Nuclear Engineering and Design 210, pp. 95-123.
14. Bubelis, E., Tosello, A., Pfrang, W., Schikorr, M., Mikityuk, K., Panadero, A.L., Martorell, S., Ordóñez, J., Seubert, A., Lerchl, G., Stempniewicz, M., Alcaro, F., De Geus, E., Delmaere, T., Poumerouly, S., Wallenius, J., 2017. System codes benchmarking on a low sodium void effect

SFR heterogeneous core under ULOF conditions. Nuclear Engineering and Design 320, pp. 325-345.

15. P. Sciora et.al., “Analysis of the Superphenix start-up tests with APOLLO-3: From zero power isothermal conditions to dynamic power transient analysis”, The European Physical Journal Conferences, January 2021, DOI: 10.1051/epjconf/202124706044.
16. E.-Y. Garcia-Cervantes, “Modeling and analysis of power fast reactors tests for the neutronic calculation scheme APOLLO-3®-SFR applied to the ASTRID reactor”, Doctoral thesis, 2019
17. Austregesilo, H., Bals, C., Hora, A., Lerchl, G., Romestedt, P., Schöffel, P., von der Cron, D., Weyermann, F., 2016. ATHLET 3.1A Models and Methods 4.
18. Zhou, C., Huber, K., Cheng, X., 2013. Validation of the modified ATHLET code with the natural convection test of the PHENIX reactor. Annals of Nuclear Energy 59, pp. 31–46.
19. Di Nora, V.A., Fridman, E., Mikityuk, K., 2019. Benchmarking ATHLET against TRACE as applied to Superphénix start-up tests, in Proc.: International Congress on Advances in Nuclear Power Plants - ICAPP2019, 12.-15.05.2019, Juan-Les-Pins, France, Juan-les-Pins, France.
20. “Fast Reactor Database. 2006 Update”, IAEA-TECDOC-1531, IAEA, December 2006.
21. J. Gourdon, B. Mesnage, J. L. Voitellier and M. Suescun, “An Overview of Superphenix Commissioning Tests”, Nuclear Science and Engineering, 106, pp. 11-17 (1990).